J. Fluid Mech. (1998), *vol.* 362, *pp.* 17–51. Printed in the United Kingdom

© 1998 Cambridge University Press

The effects of rotation on axisymmetric gravity currents

By MARIUS UNGARISH† AND HERBERT E. HUPPERT

Institute of Theoretical Geophysics, Department of Applied Mathematics and Theoretical Physics, University of Cambridge, Silver Street, Cambridge CB3 9EW, UK.

(Received 29 May 1997 and in revised form 12 December 1997)

Axisymmetric gravity currents in a system rotating around a vertical axis, that result when a dense fluid intrudes horizontally under a less dense ambient fluid, are studied. Situations for which the density difference between the fluid is due either to compositional differences or to suspended particulate matter are considered. The fluid motion is described theoretically by the inviscid shallow-water equations. A 'diffusion' equation for the volume fraction in the suspension is derived for the particle-driven case, and two different models for this purpose are presented. We focus attention on situations in which the apparent importance of the Coriolis terms relative to the inertial terms, represented by the parameter $\mathscr{C}$ (the inverse of a Rossby number), is not large. Numerical and asymptotic solutions of the governing equations clarify the essential features of the flow field and particle distribution, and point out the striking differences from the non-rotating case (Bonnecaze, Huppert & Lister 1995). It is shown that the Coriolis effects eventually become dominant; even for small $\mathscr{C}$, Coriolis effects are negligible only during an initial period of about one tenth of a revolution. Thereafter the interface of the current acquires a shape which has a downward decreasing profile at the nose and its velocity of propagation begins to decrease to zero more rapidly than in the non-rotating situation. This relates the currents investigated here to the previously studied quasi-steady oceanographic structures called rings, eddies, vortices or lenses, and may throw additional light on the dynamics of their formation. The theoretical results were tested by some preliminary experiments performed in a rotating cylinder of diameter 90 cm filled with a layer of water of depth 10 cm in which a cylinder of heavier saline fluid of diameter 9.4 cm was released.

1. Introduction

Gravity currents occur whenever fluid of one density flows primarily horizontally into fluid of a different density. Many such situations arise in both industrial and natural settings, as reviewed by Simpson (1997). Commonly the current is driven by compositional or temperature differences, to lead to a homogeneous current, or by suspended particulate matter, to lead to a particle-driven current. Combinations of both particle and compositional or temperature differences can also occur (Sparks *et al.* 1993). Currents may propagate in either a two-dimensional or axisymmetric configuration, or may be otherwise influenced by side and/or topographic constraints. Some of these processes have now been fairly well investigated. Our aim here is

† Present address: Department of Computer Science, Technion, Haifa 32000, Israel.

https://doi.org/10.1017/S0022112098008878 Published online by Cambridge University Press

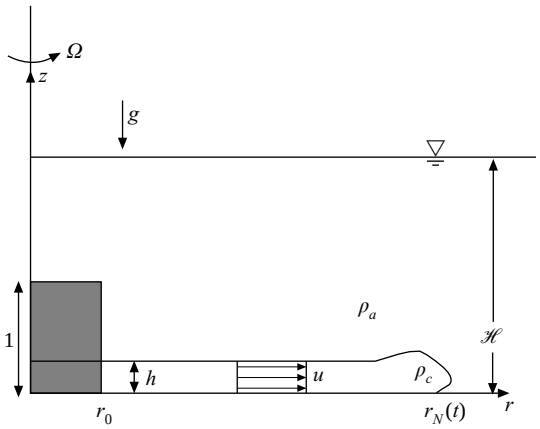


FIGURE 1. Schematic description of the system; z is the axis of symmetry. The grey region represents the current at $t = 0$, and the initial height is used as the length scale. The deformation of the upper interface is negligible small.

primarily to evaluate the effects of rotation on the propagation and shape of high-Reynolds-number homogeneous and particle-driven gravity currents of finite volume in an axisymmetric geometry. Rotational effects can play a role in industrial settings and will definitely play a major role in many large-scale natural situations. Gravity currents of fixed volume in a rotating frame have been investigated in configurations with a sidewall that prevents free azimuthal motion and hence axisymmetry, a topic reviewed by Griffiths (1986). The novel features of the gravity current investigated here are the axial symmetry of the configuration and the incorporation of the particle-drive mechanism. In these respects, the work presented herein can be viewed as an extension to the new approach taken to balancing inertial, buoyancy and particle effects in flows by Bonnecaze, Huppert & Lister (1993) and Bonnecaze *et al.* (1995). Closely related investigations concerning a possible steady-state attained by density-driven rotating axisymmetric currents and their stability were performed by Saunders (1973), Csanady (1979), Flierl (1979) and Griffiths & Linden (1981) as detailed below.

The system under consideration is sketched in figure 1: a deep layer of ambient fluid, of density ρ_a, above a solid horizontal surface at $z = 0$, is in solid-body rotation with angular velocity Ω about the vertical axis of symmetry. At time $t = 0$ a fixed volume of co-rotating heavier fluid, initially in a cylinder of height h_0 and radius $r_0 h_0$, where r_0 is dimensionless, is released into the ambient fluid. An axisymmetric current starts to spread radially. If the current fluid is a mixture (suspension) of heavier particles in essentially the same interstitial fluid as the ambient, this is called a particle-driven current; while the current spreads, particles settle out and the effective strength of the current, as compared with a homogeneous current, decays.

The corresponding flow in a non-rotating system was studied by Bonnecaze *et al.* (1995). Our task here is to incorporate the Coriolis effects into the modelling of that flow and to understand their major influence. Loosely speaking, the azimuthal velocity, with an appropriate equation, must be added to the previously studied system. It turns out that this has non-trivial consequences.

In a non-rotating gravity current the characteristic length is h_0, the characteristic velocity, purely in the radial direction, is $(g'h_0)^{1/2}$ and the reduced gravity is $g' = (\rho_c/\rho_a - 1)g$, where ρ_c is the density of the fluid that makes up the current and g is the acceleration due to gravity. In a particle-driven current ρ_c may vary in time due

https://doi.org/10.1017/S0022112098008878 Published online by Cambridge University Press

to the settling of particles from the suspension. Hence the initial value of g', denoted by g'_0, is used for definiteness. Using h_0 and $(g'_0 h_0)^{1/2}$ as length and velocity scales, the relevant dimensionless parameters are the initial radius, r_0 (which also determines the volume of the current) and the dimensionless particle settling velocity, β, which is assumed small. Note that by setting $\beta \equiv 0$ the homogeneous gravity current is recovered. An appropriately defined Reynolds number is assumed large, and hence viscous effects need not be incorporated.

In a current in a rotating system Coriolis effects must be accounted for. With the above-mentioned scales for length and velocity, the Coriolis effects are proportional to the dimensionless parameter

$$\mathscr{C} = \Omega(h_0/g'_0)^{1/2} = 1/Ro, \tag{1.1}$$

which expresses the ratio of the azimuthal velocity Ωh_0 to the inertial velocity $(g'_0 h_0)^{1/2}$ and can be defined as the inverse of the formal Rossby number, Ro. However, it should be noticed that Coriolis effects remain after the decay of the inertial processes. For this reason Coriolis effects may produce significant differences from non-rotating currents even for very small values of $\mathscr{C}$. The most striking difference is the existence of a finite radius of propagation. More accurate considerations, discussed below, show that if $\mathscr{C} r_0$ is small the Coriolis effects do not affect the propagation of the current much during, say, the initial tenth of a revolution of the system following the release. During this time the current attains a much larger radius than the initial one and a large lag of angular velocity relative to the ambient fluid. This and the subsequent flow may be stable for at least several revolutions of the system. On the other hand, if $\mathscr{C} r_0$ is large, the current is able to perform only a slight readjustment of its initial conditions in a boundary layer of dimensionless thickness $1/\mathscr{C}$ produced by a corresponding movement of the nose. (Note that the dimensional distance $h_0/2\mathscr{C}$, or $h_0 Ro/2$, is usually defined as the Rossby radius of deformation or adjustment.) This is, however, a very unstable situation.

Evidently, the most interesting cases – before the onset of instabilities, at least – are in the domain of small $\mathscr{C} r_0$. This also appears to be the pertinent range of some geophysical systems, such as the Gulf Stream core rings (Saunders 1973; Flierl 1979; Csanady 1979). Indeed, the axisymmetric rotating currents of the present investigation are closely related to structures called rings, vortices, eddies or lenses of one fluid embedded in a fluid of a different density in a rotating frame. These structures are quasi-steady (stability disregarded): their fluid–fluid interface reflects a local equilibrium between the pressure gradient and the radial Coriolis component, while the radial motion (the azimuthal Coriolis component) is zero; we shall refer to them as SL (steady-state lens). Long-time effects, such as spin-up and/or sedimentation in the particle-driven case, will ultimately lead to the decay of a stable SL. The mechanism of formation of Gulf Stream (and other large-scale oceanographic) eddies is from meanders of the main current (as discussed by Richardson 1983), not from the idealized lock release as considered here. However, following Flierl (1979) and Csanady (1979) for example, we can argue that once an independent almost axisymmetric and non-cyclonic volume of anomalous water is formed its subsequent spread is expected to have features in common with the lock-release current.

The experiments of Saunders (1973) and, more extensively, of Griffiths & Linden (1981) concern homogeneous ($\beta = 0$) SLs and focus on questions of stability. The former study considered 'bottom vortices' produced by releasing a cylinder of heavy fluid on the flat horizontal bottom of a container of less dense fluid. The latter studied 'surface vortices' produced by an opposite set of fluids (in an open container).

https://doi.org/10.1017/S0022112098008878 Published online by Cambridge University Press

Saunders reported stable SLs for $\mathscr{C}r_0 < 0.4$. The SLs of Griffiths & Linden were always unstable, but for $\mathscr{C}r_0 < 1$ the instability seemed to become significantly large only several revolutions after the establishment of a lens shape. Griffiths & Linden (1981) attribute the stability of the bottom vortices to the action of the viscous Ekman layer at the bottom, which may be able to suppress the growth of the disturbances, in contrast to the situations of surface vortices. The instabilities were found to be predominantly baroclinic when the thickness of the vortex is larger than 0.1 of the maximal depth of the ambient fluid, but predominantly barotropic otherwise.†

It is emphasized that these experimental studies, as well as the theoretical ones (Flierl 1979; Csanady 1979, to be discussed in §3), considered the problem from the quasi-steady point of view. The dynamic process of the gravity current that connects simple initial conditions to an SL has not been investigated.

The present work attempts to throw some light on the propagation of a gravity current from an initially simple state – actually, the one used in the above-mentioned experiments – to the attainment of a (quasi) maximal radius of spread, where the thickness of the head is reduced to zero, which is shown to be close to the SL, in the parametric range of small $\mathscr{C}$. In particular, our investigation is concerned with particle-driven currents. In §2 the model equations of motion, based on shallow-water approximations, and the appropriate boundary conditions are introduced. The SL solution of these equations is briefly presented in §3. Some numerical results of the rotating gravity currents are presented in §4, and their difference from the non-rotating case emphasized. A better insight is sought in §5 via an analytical approximate solution, for small $\mathscr{C}$ and β, which is supported by additional numerical results. A discussion of our preliminary experimental investigations is presented in §6.

2. Formulation

Consider an ambient fluid of constant density, ρ_a. The fluid making up the current, see figure 1, is considered to be a monodispersed suspension in which the particles occupy the volume fraction α, with initial value α_0. We denote by subscripts i the continuous or interstitial fluid in the suspension, p the dispersed or particle phase, and define the density parameters

$$\varepsilon = \frac{\rho_p - \rho_i}{\rho_i} \quad \text{and} \quad \gamma = \frac{\rho_a - \rho_i}{\varepsilon\alpha_0\rho_i} = \frac{1}{\alpha_0}\frac{\rho_a - \rho_i}{\rho_p - \rho_i}. \tag{2.1}$$

The effective density of the suspension making up the current is given by the simple combination of the density of the components,

$$\rho_c = (1-\alpha)\rho_i + \alpha\rho_p = \rho_i + \alpha(\rho_p - \rho_i) = \rho_i(1+\varepsilon\alpha). \tag{2.2}$$

The initial reduced gravity of the current is defined by

$$g_0' = \left[\frac{\rho_c(t=0)}{\rho_i} - 1\right] g = \varepsilon\alpha_0 g. \tag{2.3}$$

If the current is homogeneous, or the particle volume fraction remains constant, the effective reduced gravity remains g_0'.

We assume that the initial mass concentration of the particles is small and so $\varepsilon\alpha_0 \ll 1$. We note that the subsequent analysis can be readily reduced to that of a

† The parameter θ or θ_0 (defined as the Richardson number) in these papers is equal to $1/(2\mathscr{C}r_0)^2$ in this paper.

https://doi.org/10.1017/S0022112098008878 Published online by Cambridge University Press

homogeneous-density-current case with a given g_0'; in this case, the equation for the volume fraction should be discarded (and α set formally equal to α_0).

We use a cylindrical coordinate system rotating with angular velocity Ω around the vertical axis of symmetry, z. The (mass averaged) velocity vector is denoted by $\boldsymbol{v} = \{u, v, w\}$ and the gravity acceleration by $-g\hat{z}$. The equations of motion for a suspension contain some additional terms over the more familiar Navier–Stokes equations for a homogeneous fluid, as explained, for example, by Ungarish (1993). However, when the relative particle velocity, $\boldsymbol{v}_R$, is small compared to the fluid velocity and the relative density difference between the suspension and the pure fluid, $\varepsilon\alpha_0$, is also small, these differences may be neglected. This approximation is employed here. Thus, the inviscid axisymmetric equations of motion, valid in both suspension and pure fluid regions, are the continuity equation,

$$\nabla \cdot \boldsymbol{v} = \frac{1}{r}\frac{\partial}{\partial r}ur + \frac{\partial w}{\partial z} = 0, \tag{2.4}$$

and the momentum balances in the radial, azimuthal and axial directions,

$$\rho\left[\frac{\partial u}{\partial t} + \frac{1}{r}\frac{\partial}{\partial r}ru^2 + \frac{\partial}{\partial z}uw - v\left(2\Omega + \frac{v}{r}\right) - \Omega^2 r\right] = -\frac{\partial p}{\partial r}, \tag{2.5}$$

$$\rho\left[\frac{\partial v}{\partial t} + \frac{1}{r}\frac{\partial}{\partial r}ruv + \frac{\partial}{\partial z}vw + u\left(2\Omega + \frac{v}{r}\right)\right] = 0, \tag{2.6}$$

and

$$\rho\left[\frac{\partial w}{\partial t} + u\frac{\partial w}{\partial r} + w\frac{\partial w}{\partial z}\right] = -\frac{\partial p}{\partial z} - \rho g, \tag{2.7}$$

where the value of ρ in these equations should be taken as ρ_a in the ambient and ρ_c in the domain of the current, see (2.2).

In addition, in the suspension region a transport (or 'diffusion') equation for the dispersed particles is needed. This will be introduced later. Two models for the particle distribution inside the suspending fluid are considered.

(*a*) Model T, for turbulent remixing, assumes that all the fluid of the initial current remains part of the current, in the axial domain $0 \leqslant z \leqslant h(r,t)$. The dispersed particles settle out from the current only at the bottom with constant dimensionless velocity $-\beta\hat{z}$ calculated from the Stokes formula (hindrance may be incorporated). The remaining non-settled particles are remixed vertically in the current, so that the volume fraction is homogeneous in the z-direction. At the interface $z = h(r,t)$ there is no relative motion between the current and the particles.

(*b*) Model L, for laminar sedimentation, assumes that the relative velocity of the particles in the suspending fluid is $-\beta\hat{z}$ everywhere, like in a quiescent settling tank. The upper interface of the current is defined now by the kinematic shock which follows the boundary between the particles and the domain of the 'pure fluid'. By this process some of the interstitial fluid of the current is left behind the interface and becomes part of the embedding ambient fluid. From another point of view, while particles leave the current at the bottom, clear fluid leaves the current at the top.

Model T has been independently introduced by Einstein (1968), Martin & Nokes (1988) and others. Although its rigorous derivation is lacking, this model has been used with increasing confidence by various researchers. In particular Bonnecaze *et al.* (1993, 1995) used this model for a problem closely related to the present one, and showed that the theoretical predictions yielded good agreement with measurements on the distance of propagation of the current versus time and sediment deposited

https://doi.org/10.1017/S0022112098008878 Published online by Cambridge University Press

versus distance. However, no measurements of the volume fraction of particles within the flow are available for more complete validations. In a rotating current the propagation is hindered by Coriolis effects, and hence the vigour of turbulence may decrease with time and model L may become more relevant. However, for small values of β, as considered here, the difference between the two models in the main stage of propagation is expected to be small. This compatibility between the models is confirmed by the results presented later.

For the ambient fluid domain, where $\rho = \rho_a$ and $\alpha = 0$, we assume that $u = v = w = 0$. Hence the governing equations (2.5)–(2.7) indicate that

$$p = \rho_a \left(\tfrac{1}{2}\Omega^2 r^2 - gz\right) + \text{const.} \tag{2.8}$$

Next, consider the domain of the current, $0 \leqslant z \leqslant h(r,t)$ for $r \leqslant r_N(t)$. Here the 'shallow-water' approximation is introduced. This leads to the argument that the left-hand side of the vertical momentum equation (2.7) is small and hence (2.7) can be integrated to yield

$$p = -\rho_i g z - \rho_i \varepsilon \int_0^z \alpha(r, z', t)\mathrm{d}z' + f(r,t), \tag{2.9}$$

where (2.2) was used for the density in this region. At the interface $z = h(r,t)$ between the current and the ambient fluid, the continuity of pressure evaluated from (2.8) and (2.9) specifies $f(r,t)$. After some arrangement, we obtain for the current domain

$$p = \tfrac{1}{2}\rho_a \Omega^2 r^2 + \rho_i g \left[\left(1 - \frac{\rho_a}{\rho_i}\right) h + \varepsilon \int_z^h \alpha(r, z', t)\mathrm{d}z' - z\right] + \text{const}, \tag{2.10}$$

and

$$\frac{\partial p}{\partial r} = \rho_a \Omega^2 r + \rho_i g \left[\left(1 - \frac{\rho_a}{\rho_i}\right) \frac{\partial h}{\partial r} + \varepsilon \int_z^h \frac{\partial \alpha(r, z', t)}{\partial r}\mathrm{d}z' + \varepsilon\alpha \frac{\partial h}{\partial r}\right], \tag{2.11}$$

where α is taken at $z = h$. Subsequently, the governing equations in the region of the current are z-averaged, and reduced to equations for the z-averaged variables u, v, α. Some details are given in the Appendix.

Hereafter, in the spirit of the 'shallow-water' framework, the z-averaged variables u, v, α are considered as functions of r and t only. The resulting equations for these variables are presented below, in dimensionless form, after scaling, by the following relationships:

$$\{r, z, t, u, v, \alpha\} = \{h_0 r, h_0 z, T_{ref} t, U_{ref} u, \mathscr{C} U_{ref} v, \alpha_0 \phi\}, \tag{2.12}$$

where

$$U_{ref} = (h_0 g_0')^{1/2}, \quad T_{ref} = (h_0/g_0')^{1/2}, \quad \mathscr{C} = \Omega (h_0/g_0')^{1/2}. \tag{2.13}$$

Here h_0 is the initial height of the current, and U_{ref} and T_{ref} are the conventional scales used in non-rotating gravity current problems. The Stokes settling velocity of the particles, scaled by U_{ref}, is denoted by β. Note that in this scaling the number of revolutions performed by the rotating frame during time t is $\mathscr{C}t/2\pi$, therefore another time coordinate, $\tau = \mathscr{C}t$, will become relevant when considering effects associated with the rotation.

The parameter $\mathscr{C}$ represents the importance of Coriolis effects relative to inertial ones and can be considered as the inverse of the Rossby number of the flow. We are concerned with flows with small $\mathscr{C}$ (or rather, small $\mathscr{C}r_0$, where r_0 is the dimensionless initial radius).

https://doi.org/10.1017/S0022112098008878 Published online by Cambridge University Press

We keep in mind that the geometry and flow field of the current undergo big changes in the process under investigation and therefore the scaled variables are not always of order unity. The scaling velocity U_{ref} is representative of the initial stage of the motion, which is controlled by a buoyancy–inertia balance in a layer of height h_0 and gravity excess g_0'; the nose very rapidly acquires a radial velocity of this order of magnitude. The azimuthal velocity and length scalings reproduce well the angular velocity acquired after a spread to, say, twice the initial radius. When the scaled time, t, becomes large the scaled height, h, and radial velocity, u, and possibly the scaled volume fraction, ϕ, become small, but the angular velocity remains $O(1)$. These features will become more evident during the progress of the analysis. The equations of motion have been rechecked for consistency with these variations in the range of parameters presented. A convenient rescaling of the variables is discussed in Ungarish & Huppert (1998).

The equations of motion can be conveniently expressed either for h and the combined variables,

$$\varphi = \phi h, \quad q = uh, \quad \text{and } \mathscr{V} = vh, \tag{2.14}$$

in 'conservation form', or for the original variables in 'characteristic form', as follows.

2.1. *The governing equations, model T*

In conservation form the equations can be written as

$$\frac{\partial h}{\partial t} + \frac{\partial}{\partial r} uh = -\frac{uh}{r}, \tag{2.15}$$

$$\frac{\partial}{\partial t} uh + \frac{\partial}{\partial r}\left[u^2 h + \tfrac{1}{2}(\phi - \gamma)h^2\right] = -\frac{u^2 h}{r} + \mathscr{C}^2 vh\left(2 + \frac{v}{r}\right), \tag{2.16}$$

$$\frac{\partial}{\partial t}\phi h + \frac{\partial}{\partial r} u\phi h = -\beta\phi - \frac{u\phi h}{r} \tag{2.17}$$

and

$$\frac{\partial}{\partial t} vh + \frac{\partial}{\partial r} uvh = -2uh\left(1 + \frac{v}{r}\right). \tag{2.18}$$

In characteristic form, this becomes

$$\begin{bmatrix} h_t \\ u_t \\ \phi_t \\ v_t \end{bmatrix} + \begin{bmatrix} u & h & 0 & 0 \\ (\phi - \gamma) & u & \frac{1}{2}h & 0 \\ 0 & 0 & u & 0 \\ 0 & 0 & 0 & u \end{bmatrix} \begin{bmatrix} h_r \\ u_r \\ \phi_r \\ v_r \end{bmatrix} = \begin{bmatrix} -uh/r \\ \mathscr{C}^2 v(2 + v/r) \\ -\beta\phi/h \\ -u(2 + v/r) \end{bmatrix}. \tag{2.19}$$

The characteristic paths and relationships are essential for the application of boundary conditions, and can also be used for obtaining the solution numerically (see Bonnecaze *et al.* 1993 for further discussion). The standard derivation, see for example Anderson, Tannehill & Pletcher (1984), requires first the eigenvalues of the matrix of coefficients, which are

$$\lambda_+ = u + [h(\phi - \gamma)]^{1/2}, \quad \lambda_- = u - [h(\phi - \gamma)]^{1/2}, \quad \lambda_3 = u, \quad \lambda_4 = u,$$

and the corresponding eigenvectors

$$\left(1, \left(\frac{h}{\phi - \gamma}\right)^{1/2}, \frac{1}{2}\frac{h}{\phi - \gamma}, 0\right), \left(1, -\left(\frac{h}{\phi - \gamma}\right)^{1/2}, \frac{1}{2}\frac{h}{\phi - \gamma}, 0\right), (0, 0, 1, 0), (0, 0, 0, 1).$$

Consequently, the relationships between the variables on the characteristics with

https://doi.org/10.1017/S0022112098008878 Published online by Cambridge University Press

$\mathrm{d}r/\mathrm{d}t = \lambda$, are as follows:

$$\lambda_+ : \mathrm{d}h + \left(\frac{h}{\phi-\gamma}\right)^{1/2}\mathrm{d}u + \frac{1}{2}\frac{h}{\phi-\gamma}\mathrm{d}\phi = \mathrm{d}t\left[-\frac{uh}{r} + \left(\frac{h}{\phi-\gamma}\right)^{1/2}\mathscr{C}^2 v\left(2+\frac{v}{r}\right) - \frac{1}{2}\beta\frac{\phi}{\phi-\gamma}\right]; \tag{2.20}$$

$$\lambda_- : \mathrm{d}h - \left(\frac{h}{\phi-\gamma}\right)^{1/2}\mathrm{d}u + \frac{1}{2}\frac{h}{\phi-\gamma}\mathrm{d}\phi = \mathrm{d}t\left[-\frac{uh}{r} - \left(\frac{h}{\phi-\gamma}\right)^{1/2}\mathscr{C}^2 v\left(2+\frac{v}{r}\right) - \frac{1}{2}\beta\frac{\phi}{\phi-\gamma}\right]; \tag{2.21}$$

$$\lambda_3 : \mathrm{d}\phi = -\frac{\beta\phi}{h}\mathrm{d}t; \tag{2.22}$$

$$\lambda_4 : \mathrm{d}v = -u\left(2+\frac{v}{r}\right)\mathrm{d}t. \tag{2.23}$$

Further manipulation on the last characteristic yields a convenient result. Since on $\lambda_4\, u\mathrm{d}t = \mathrm{d}r$, (2.23) can be rewritten as

$$\frac{\mathrm{d}v}{\mathrm{d}r} + \frac{v}{r} = -2.$$

With the initial condition $v = 0$ at $r = r_{init}$, this has the solution

$$v = -r\left[1 - \left(\frac{r_{init}}{r}\right)^2\right]. \tag{2.24}$$

In particular, at the nose

$$v(r = r_N) = -r_N(t)\left(1 - \left[r_0/r_N(t)\right]^2\right). \tag{2.25}$$

Note that the angular velocity tends quickly to -1 as the current spreads away from its initial $r_N(0) = r_0$ state, a manifestation of the potential-vorticity conservation as shown below.

2.2. *The governing equations, model L*

In conservation form the equations can be written as

$$\frac{\partial h}{\partial t} + \frac{\partial}{\partial r}uh = -\frac{uh}{r} - \beta, \tag{2.26}$$

$$\frac{\partial}{\partial t}uh + \frac{\partial}{\partial r}\left[u^2 h + \tfrac{1}{2}(\phi-\gamma)h^2\right] = -\frac{u^2 h}{r} + \mathscr{C}^2 vh\left(2+\frac{v}{r}\right) - \beta u, \tag{2.27}$$

$$\frac{\partial}{\partial t}\phi h + \frac{\partial}{\partial r}u\phi h = -\beta\phi - \frac{u\phi h}{r} \tag{2.28}$$

and

$$\frac{\partial}{\partial t}vh + \frac{\partial}{\partial r}uvh = -2uh\left(1+\frac{v}{r}\right) - \beta v. \tag{2.29}$$

Note that the last term in (2.26) represents the additional settling of the interface due to the local sedimentation of the particles relative to the fluid. As a consequence, the last term in (2.27) represents the loss of radial momentum, and the last term in (2.29) represents the loss of angular momentum.

https://doi.org/10.1017/S0022112098008878 Published online by Cambridge University Press

In characteristic form, this becomes

$$\begin{bmatrix} h_t \\ u_t \\ \phi_t \\ v_t \end{bmatrix} + \begin{bmatrix} u & h & 0 & 0 \\ (\phi-\gamma) & u & \frac{1}{2}h & 0 \\ 0 & 0 & u & 0 \\ 0 & 0 & 0 & u \end{bmatrix} \begin{bmatrix} h_r \\ u_r \\ \phi_r \\ v_r \end{bmatrix} = \begin{bmatrix} -uh/r - \beta \\ \mathscr{C}^2 v(2+v/r) \\ 0 \\ -u(2+v/r) \end{bmatrix}. \tag{2.30}$$

In model L, (2.28) or the third equation of (2.30) can be replaced with $\phi = 1$ or $\varphi = h$, respectively.

The eigenvalues and eigenvectors of the coefficient matrix are as in the previous model. On characteristics $\mathrm{d}r/\mathrm{d}t = \lambda$ the following relationships hold:

$$\lambda_+ : \mathrm{d}h + \left(\frac{h}{\phi-\gamma}\right)^{1/2} \mathrm{d}u + \tfrac{1}{2}\frac{h}{\phi-\gamma}\mathrm{d}\phi = \mathrm{d}t\left[-\frac{uh}{r} + \left(\frac{h}{\phi-\gamma}\right)^{1/2} \mathscr{C}^2 v\left(2+\frac{v}{r}\right) - \beta\right], \tag{2.31}$$

$$\lambda_- : \mathrm{d}h - \left(\frac{h}{\phi-\gamma}\right)^{1/2} \mathrm{d}u + \tfrac{1}{2}\frac{h}{\phi-\gamma}\mathrm{d}\phi = \mathrm{d}t\left[-\frac{uh}{r} - \left(\frac{h}{\phi-\gamma}\right)^{1/2} \mathscr{C}^2 v\left(2+\frac{v}{r}\right) - \beta\right], \tag{2.32}$$

$$\lambda_3 : \mathrm{d}\phi = 0, \tag{2.33}$$

$$\lambda_4 : \mathrm{d}v = -u\left(2+\frac{v}{r}\right)\mathrm{d}t. \tag{2.34}$$

The result (2.25) and its derivation are also valid for this model.

2.3. *The nose boundary condition*

As in the non-rotating case, a boundary condition for the velocity at the nose, $\dot{r}_N(t)$, is essential for a proper physical definition and mathematical closure of the problem. The appropriate condition for the non-rotating case, $\mathscr{C} = 0$, has been well studied, both theoretically and experimentally, and recently extended to the particle-driven situation (see Bonnecaze *et al.* 1993, 1995). The pertinent result is that

$$\dot{r}_N = Fr(h_N\phi_N)^{1/2}, \tag{2.35}$$

$$\begin{aligned} Fr &= 1.19, \qquad 0 \leqslant h/\mathscr{H} \leqslant 0.0742 \\ &= 0.5h^{-1/3}, \quad 0.0742 \leqslant h/\mathscr{H} \leqslant 1, \end{aligned} \tag{2.36}$$

where $\mathscr{H}$ is the (dimensionless) height of the layer of ambient fluid.

For a rotating axisymmetric current, $\mathscr{C} > 0$, to the best of our knowledge no investigation on the nose condition has been performed. It can be argued heuristically that (2.35) is determined by local inertial–pressure effects in the close proximity of the nose which will be only slightly influenced by the rotation of the system if the local Rossby number is large, i.e. $\mathscr{C}$ is small. Indeed, we can compare the orders of magnitude of the terms (in dimensional form) $u\partial u/\partial r$ to $2\Omega v$ at $r \approx r_N$. With the anticipation that $u \sim \dot{r}_N \sim (h_N\phi_N)^{1/2}(g_0'h_0)^{1/2}$, the radial scale of variation is similar to the height, and $v \sim \Omega r_N$, so the ratio between the inertial and Coriolis terms is $\sim \phi_N/\mathscr{C}^2 r_N$ (in dimensionless form). More rigorously, using the approach of Benjamin (1968) in a rotating system, we estimate that the effect of

https://doi.org/10.1017/S0022112098008878 Published online by Cambridge University Press

rotation will introduce into the right-hand side of (2.35) a multiplication factor of the form $(1 - c\,\mathscr{C}^2 r_N/\phi_N)^{1/2}$, where the positive coefficient c is of order unity, but should be determined by either a more complex analysis or experiments. Since our investigation is concerned with small values of $\mathscr{C}$, in the absence of more accurate information, we shall proceed under the assumption that (2.35) and (2.36) remain a good approximation for rotating gravity currents. The verification, extension and improvement of this assumption is left for a separate investigation. Here some support to our approach is provided by the experiments reported in §6, which indicate good agreement between theory and measurements of $r_N(t)$ for $0 \leqslant \mathscr{C}^2 \leqslant 0.1$. We note in passing that the Coriolis effect on the nose condition is expected to be different in an axisymmetric current than in a current adjacent to a meridional wall (of the type considered, for example, by Griffiths & Hopfinger 1983 and reviewed by Griffiths 1986).

2.4. *Potential vorticity*

2.4.1. *Model T*

The potential vorticity, $(2\Omega + \hat{\boldsymbol{z}} \cdot \nabla \boldsymbol{v})/h$ (in dimensional form, or $\mathscr{C}(2 + \hat{\boldsymbol{z}} \cdot \nabla \boldsymbol{v})/h$ in dimensionless form) is conserved under the assumptions of model T. This result can be derived as follows.

We first combine (2.15) with (2.18) to obtain

$$\frac{\partial v}{\partial t} + u\left(\frac{1}{r}\frac{\partial}{\partial r} rv + 2\right) = 0. \tag{2.37}$$

Applying the operator $(1/r)\,(\partial/\partial r r)$ to the last equation, and letting

$$\zeta = \hat{z} \cdot \nabla \times \boldsymbol{v} = \frac{1}{r}\frac{\partial}{\partial r} rv,$$

we obtain, after some rearrangement, that

$$\frac{\partial(\zeta + 2)}{\partial t} + u\frac{\partial}{\partial r}(\zeta + 2) + (\zeta + 2)\frac{1}{r}\frac{\partial}{\partial r} ru = 0, \tag{2.38}$$

or

$$\frac{\mathrm{D}}{\mathrm{D}t}(\zeta + 2) = -(\zeta + 2)\frac{1}{r}\frac{\partial}{\partial r} ru. \tag{2.39}$$

Note that (2.15) can be expressed as

$$h\frac{1}{r}\frac{\partial}{\partial r} ru = -\left(\frac{\partial h}{\partial t} + u\frac{\partial h}{\partial r}\right) = -\frac{\mathrm{D}h}{\mathrm{D}t}. \tag{2.40}$$

Dividing (2.39) by h and substituting (2.40), we obtain

$$\frac{\mathrm{D}}{\mathrm{D}t}\left(\frac{\zeta + 2}{h}\right) = 0. \tag{2.41}$$

Initially, for all the fluid 'particles' in our problem, $\zeta = 0$ and $h = 1$ and therefore

$$h(r, t) = 1 + \tfrac{1}{2}\zeta(r, t) = 1 + \frac{1}{2}\frac{1}{r}\frac{\partial}{\partial r} rv(r, t) = 1 + \omega + \frac{1}{2} r\frac{\partial \omega}{\partial r}. \tag{2.42}$$

Consider now volume conservation, which in view of (2.42) becomes

$$\pi r_0^2 = 2\pi \int_0^{r_N} h r \mathrm{d}r = 2\pi \int_0^{r_N} \left[1 + \frac{1}{2}\frac{1}{r}\frac{\partial}{\partial r} rv\right] r \mathrm{d}r = \pi \left[r_N^2 + r_N v(r_N, t)\right],$$

https://doi.org/10.1017/S0022112098008878 Published online by Cambridge University Press

which yields the condition

$$\omega(r_N, t) = -1 + \left[\frac{r_0}{r_N(t)}\right]^2. \tag{2.43}$$

This is identical with (2.25), which was obtained from different considerations.

The combination of (2.42) and (2.43),

$$h(r_N) = \left(\frac{r_0}{r_N}\right)^2 + \tfrac{1}{2} r_N \left(\frac{\partial \omega}{\partial r}\right)_N,$$

has important implications: if $(\partial\omega/\partial r)_N < 0$, $h(r_N)$ decreases with the propagation faster than expected from continuity considerations, and may even vanish. This is of course accompanied by a diminution of the head velocity, $\dot{r}_N$. We shall see that, even for small values of $\mathscr{C}$, the radial motion may stop when $r_N \sim O(\mathscr{C}^{-1/2} r_0)$ is reached (for larger values of $\mathscr{C}$ the departure from r_0 is much smaller).

2.4.2. *Model L*

Equations (2.37)–(2.39) remain unchanged, but in this case

$$h \frac{1}{r} \frac{\partial}{\partial r} ru = -\left(\frac{\partial h}{\partial t} + u \frac{\partial h}{\partial r}\right) - \beta = -\frac{\mathrm{D}h}{\mathrm{D}t} - \beta. \tag{2.44}$$

Therefore, proceeding as before, we obtain

$$\frac{\mathrm{D}}{\mathrm{D}t}\left(\frac{\zeta + 2}{h}\right) = \frac{\beta}{h} \frac{\zeta + 2}{h}, \tag{2.45}$$

or

$$\frac{\mathrm{D}}{\mathrm{D}t} \ln\left(\frac{\zeta + 2}{h}\right) = \frac{\beta}{h}. \tag{2.46}$$

3. Steady-state lens shape (SL)

If $\beta = 0$ equations (2.15)–(2.18) admit a non-trivial steady-state solution with $u = 0$ and ϕ constant. The relevance to the rotating gravity current is evident: we expect that in stable circumstances the time-dependent motion tends to a similar steady state (or quasi-steady state in more realistic circumstances, as explained below).

This steady state has been considered by Flierl (1979) and Csanady (1979) in the context of warm core rings in oceans. There are, however, differences with their solutions. We obtained approximate analytical solutions for both small and large values of $\mathscr{C} r_0$; Csanady also presented analytical solutions but linearized the right-hand side of (3.1), replacing $2 + \omega$ by 2, which can be justified only for large values of $\mathscr{C} r_0$ (Csanady's $h(0)$ is about twice as large as the correct value for small $\mathscr{C} r_0$). We obtained numerical solutions essentially similar to those of Flierl (1979), but with different scalings; Flierl focused attention on the parameters at the final shape, while we define the results using the parameters at the initial state. We note in passing that the 'Rossby number' ϵ defined by Flierl is equivalent to $\mathscr{C}[-1+(r_0/r_N)^2]$ in the present notation, and the 'Rossby radius' R is $h_0/2\mathscr{C}$ in the present notation. The major novel information gained in this work, however, concerns the dynamic development of the SL, as considered below.

For simplicity, take $\phi - \gamma = 1$, i.e. the relative difference between the densities of

https://doi.org/10.1017/S0022112098008878 Published online by Cambridge University Press

the current and the ambient fluid is $\varepsilon\alpha_0$, equal to the ratio g_0'/g. To obtain $h(r)$ and $\omega(r)$ at steady state we may use the radial momentum balance (2.16),

$$\frac{\mathrm{d}h}{\mathrm{d}r} = \mathscr{C}^2 r\omega(2+\omega), \tag{3.1}$$

and the potential vorticity conservation in form (2.42),

$$h = 1 + \frac{1}{2}\frac{1}{r}\frac{\mathrm{d}}{\mathrm{d}r}r^2\omega. \tag{3.2}$$

Substitution of (3.2) into (3.1) gives a single equation for ω

$$\frac{\mathrm{d}}{\mathrm{d}r}\frac{1}{r}\frac{\mathrm{d}}{\mathrm{d}r}r^2\omega = 2\mathscr{C}^2 r\omega(2+\omega), \tag{3.3}$$

with the boundary conditions

$$\omega = -1 + (r_0/r_N)^2 \text{ and } h = 0 \quad (r = r_N). \tag{3.4}$$

The latter condition is necessary for consistency with $u_N = 0$, but r_N is not yet known. Note that (3.1) and (3.2) also imply $\mathrm{d}\omega/\mathrm{d}r = 0$ at $r = 0$.

It is convenient to define $y = r/r_N$ and to reformulate (3.2) and (3.3) as

$$\frac{\mathrm{d}^2\omega}{\mathrm{d}y^2} + \frac{3}{y}\frac{\mathrm{d}\omega}{\mathrm{d}y} - 2\mathscr{C}^2 r_N^2\omega(2+\omega) = 0 \tag{3.5}$$

and

$$h = 1 + \omega + \frac{1}{2}y\frac{\mathrm{d}\omega}{\mathrm{d}y}. \tag{3.6}$$

The associated boundary conditions are

$$\omega = -1 + (r_0/r_N)^2 \quad (y = 1); \quad \frac{\mathrm{d}\omega}{\mathrm{d}y} = 0 \quad (y = 0); \tag{3.7}$$

$$1 + \omega + \frac{1}{2}\frac{\mathrm{d}\omega}{\mathrm{d}y} = 0 \quad (y = 1). \tag{3.8}$$

From (3.6) the last condition imposes $h(y = 1) = 0$.

3.1. *Solutions*

3.1.1. $\mathscr{C}r_0 \ll 1$

Assuming an expansion of ω in powers of $\mathscr{C}r_N$ (or of $\mathscr{C}r_0$), we readily verify that

$$r_N = \mathscr{C}^{-1/2}(2r_0)^{1/2}, \tag{3.9}$$

$$\omega = -1 + \mathscr{C}r_0 - \tfrac{1}{4}\mathscr{C}^2 r^2 = -1 + \mathscr{C}r_0(1 - \tfrac{1}{2}y^2), \tag{3.10}$$

$$h = \tfrac{1}{2}\mathscr{C}^2(r_N^2 - r^2) = \mathscr{C}r_0(1 - y^2) \tag{3.11}$$

are the leading terms that satisfy the equation and the boundary conditions (with a relative error $O[(\mathscr{C}r_0)^2]$). (It is evident that the term $2 + \omega$ in this case is close to 1.)

The striking outcome is the quite small radius of spreading of the 'current', even for small $\mathscr{C}$ (recall that in a non-rotating frame a similar current will spread, theoretically, to infinity). Although the Coriolis effects enter the equations formally with the

https://doi.org/10.1017/S0022112098008878 Published online by Cambridge University Press

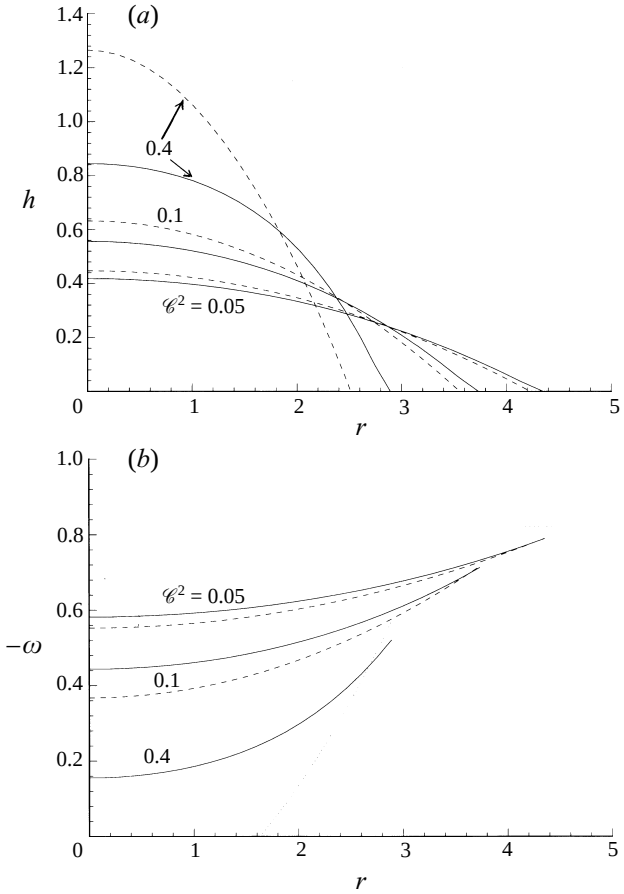


FIGURE 2. Steady lens, numerical (—) and approximate (– – –) solutions for various $\mathscr{C}^2$, $r_0 = 2$. (*a*) h vs. r; (*b*) ω vs. r.

coefficient $\mathscr{C}^2$, they actually affect the azimuthal velocity to $O(\mathscr{C})$ and radial motion to $O(\mathscr{C}^{1/2})$.

We also remark that the current spreads only $(\mathscr{C}r_0/2)^{1/2}$ times the Rossby radius of deformation, $h_0/2\mathscr{C}$.

The time of propagation of the nose from the initial to the final position given by (3.9) is $O(\mathscr{C})$, or, in dimensional form, $O(\Omega^{-1})$. Thus, such a lens-shape steady structure may develop during the first revolution of the rotating frame, on the same time scale as the formation of the Ekman layers. The essential dynamics of the establishment of the lens is discussed later.

Additional support to the present approximation is gained by comparison with the numerical solution of the equations governing the SL. We use centred finite differences on a uniform grid. For given $\mathscr{C}$ and r_0 we estimate r_N^2 and solve (3.5) subject to (3.7). Iterations are performed on the nonlinear term $\omega(2+\omega)$, starting with the value of $\omega(y=1)$. We correct the estimate to r_N until (3.8) is satisfied.

Results are given in figure 2 for $r_0 = 2$, $\mathscr{C}^2 = 0.05$, 0.1 and 0.4. The numerical results are in good agreement with the approximations (3.9)–(3.11) for the first two values of $\mathscr{C}^2$ (actually, $\mathscr{C}^2 r_0^2 = 0.2$ and 0.4).

https://doi.org/10.1017/S0022112098008878 Published online by Cambridge University Press

3.1.2. $\mathscr{C}r_0 \gg 1$

For $\mathscr{C}r_N \gg 1$, the rotational effects are expected to dominate and hence the radial motion is strongly restricted. An inspection of (3.5) indicates that when the coefficient $\mathscr{C}r_N \gg 1$, ω is small and has a boundary-layer structure. Using an expansion in powers of $(1/\mathscr{C}r_N)$ (or $(1/\mathscr{C}r_0)$), we obtain the leading terms

$$r_N = r_0\left(1 + \frac{1}{2\mathscr{C}r_N}\right), \tag{3.12}$$

$$\omega = -\frac{1}{\mathscr{C}r_N}\exp[2\mathscr{C}r_N(y-1)], \tag{3.13}$$

$$h = 1 - \exp[2\mathscr{C}r_N(y-1)]. \tag{3.14}$$

The agreement with Csanady's solution is good because the present small ω vindicates the approximation $2 + \omega \approx 2$. In this range of the parameter $\mathscr{C}r_0$ the current spreads one Rossby radius.

The SL structure, even if stable, is only an approximation to real circumstances for a limited period of time. Evidently, even small viscous effects (loosely speaking, Ekman layers) will eventually smooth out the discrepancy of angular velocity between the lens and the ambient and/or solid bottom. In this respect, the SL derived for a homogeneous ($\beta = 0$) case can also be considered as an approximation for a limited period of time to a particle-driven case provided that the particles settle out more slowly than the formation process; the relevant more quantitative consideration will be given in §5. It will be shown below that a lock-released gravity current tends to an SL structure in less than one revolution of the system; on the other hand, the mechanisms that dissipate the SL may require many revolutions.

4. Numerical results

The governing equations (2.15)–(2.18) or (2.26)–(2.29) are formulated in conservation form for the variables $h, q = uh, \varphi = \phi h, \mathscr{V} = vh$. Following closely the approach of Bonnecaze *et al.* (1993, 1995), we performed the numerical solution using a finite-difference, two-step Lax–Wendroff method. To facilitate the implementation of the boundary conditions the r-coordinate was mapped into $y = r/r_N(t)$, which keeps the current in the domain $0 \leqslant y \leqslant 1$. Consequently the original equations were subjected to the following modifications:

$$\left(\frac{\partial}{\partial t}\right)_r = \left(\frac{\partial}{\partial t}\right)_y - y\frac{\dot{r}_N}{r_N}\left(\frac{\partial}{\partial y}\right)_t, \quad \left(\frac{\partial}{\partial r}\right)_t = \frac{1}{r_N}\left(\frac{\partial}{\partial y}\right)_t, \tag{4.1}$$

where the subscripts denote the fixed variable.

Artificial viscosity terms similar to those discussed by Bonnecaze *et al.* (1993, Appendix A) were added to the radial momentum equation.

As long as $h_N = h(y = 1, t) > 0$ the obvious boundary conditions are

$$u = v = 0 \quad (y = 0), \tag{4.2}$$

$$u = Fr\ [h(y = 1, t)\phi(y = 1, t)]^{1/2} \quad (y = 1). \tag{4.3}$$

The boundary conditions for h and ϕ at $y = 0$ and 1 and v at $y = 1$ must be calculated, for each new time step, from the balances on the characteristics $\lambda_-, \lambda_+, \lambda_3$. Note that there are differences between the models T and L in this respect.

After $h(y = 1)$ reaches zero the boundary conditions at $y = 1$ must be modified.

https://doi.org/10.1017/S0022112098008878 Published online by Cambridge University Press

Obviously, this is a special issue for the case of the rotating current, because in the non-rotating case the nose does not touch the bottom. We argue that after the nose touches the bottom the outer radius of the current represents a contact line (as opposed to the previous 'front') which is approximated by the conditions

$$\frac{\partial u}{\partial r} = 0 \; h = 0 \quad (y = 1-). \tag{4.4}$$

Viscous friction around $y = 1$ may become important because of the small thickness. Hence we cannot expect the last condition to remain accurate longer than, say, the formation time of an Ekman layer, which is, roughly, $\mathscr{C}^{-1}$ in the present scaling. Afterwards a spin-up process in the entire current must be considered; although the entire process may be long, the thinner outer regions, to which the Ekman layers convect the spun-up fluid, are expected to be affected first.

Actually, for both models T and L, it is not necessary to solve the full system of equations by the Lax–Wendroff scheme. For model L, the solution of the third equation in the system, (2.28), is simply $\varphi = h$, or $\phi = 1$. For model T the potential vorticity conservation results, see (2.42), allow a separate simplified solution of $v(y,t)$ after the calculation of $h(y,t)$; this still requires a finite-difference solution, so the practical gain is marginal, except for accuracy tests.

The numerical computations of the rotating current presented here are with the common parameters $r_0 = 2$, $\mathscr{C}^2 = 0.05$ and

$$\begin{aligned} Fr &= 1.19, \qquad 0 \leqslant h \leqslant 0.0742 \\ &= 0.5h^{-1/3}, \quad 0.0742 \leqslant h \leqslant 1; \end{aligned} \tag{4.5}$$

with $\beta = 5 \times 10^{-3}$ for the particle-driven cases, models T and L, and $\beta = 0$ for the homogeneous current.

This particular choice of r_0, Fr, β and model T were used in the computations for the non-rotating ($\mathscr{C} = 0$) axisymmetric current by Bonnecaze *et al.* (1995, figures 2 and 3); for the sake of comparison some of these results have been recomputed and shown here in figure 3. The present results, displayed in figures 4–6 point out the influences of the Coriolis effects in the same configuration, but with some mild rotation. (The wiggles near the centre at larger times are numerical perturbations that should be ignored.)

Figures 4(*a*) (i) and (ii) show the motion of the interface. The change with time of $h(r)$ is strikingly different from the non-rotating case: by $t = 2$ the leading portion of the rotating current has a 'nose-down' ($\partial h/\partial r < 0$) shape. The 'nose-down' portion increases with time; at $t = 8$ the entire current can be considered to have a negatively inclined interface, and the height of the nose is only about 15% of that of the non-rotating current at the same time. At about $t = 10$ the propagation of the rotating current stops at $r_N \approx 5.1$ (the non-rotating current attains this radius at $t \approx 7.5$, and doubles it at $t \approx 30$).

Very similar behaviour of $h(r,t)$ is seen for the particle-driven model L and for the homogeneous ($\beta = 0$) current in figures 5 and 6. Recall that in these cases the density excess of the current remains constant, $\phi = 1$. In the L model the interface descends slightly faster than in the T model; this effect is more pronounced near the centre. The propagation of the front until the maximal r_N is achieved, however, does not differ significantly between models T and L (or even the $\beta = 0$ case). This can be explained as follows. The propagation is dominated by $\dot{r}_N \propto h_N^{1/2}\phi_N^{1/2}$; the change of ϕ_N in model T is relatively small, about 10%, in this time interval, hence the much

https://doi.org/10.1017/S0022112098008878 Published online by Cambridge University Press

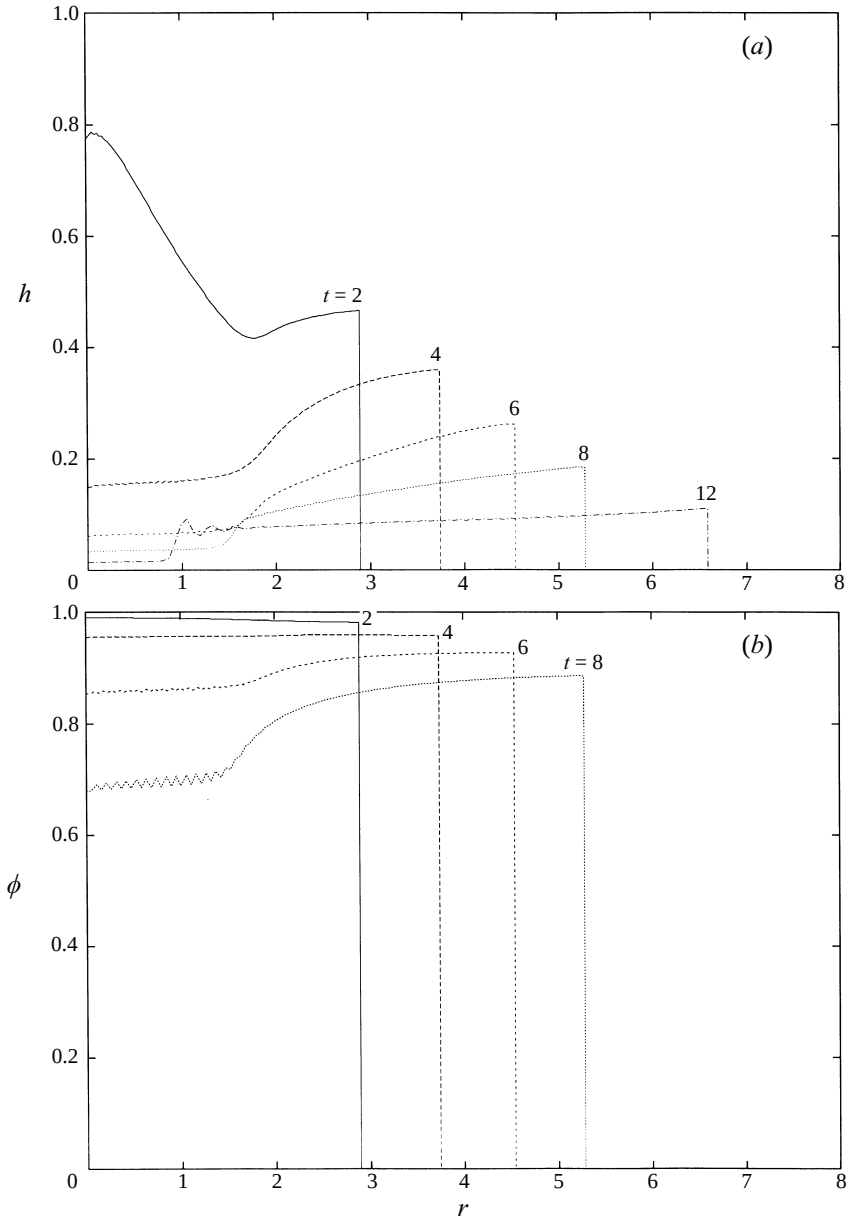


FIGURE 3. Non-rotating particle-driven current, model T, numerical results. $r_0 = 2$, $\beta = 5 \times 10^{-3}, Fr$ given by (4.5). (*a*) Interface h vs. r, various t. (*b*) Particle volume fraction ϕ vs. r, various t. (*b*) Particle volume fraction ϕ vs. r, various t.

larger variation of h_N, imposed by inertial and Coriolis effects, dominate the motion of the nose.

The global volume of the fluid in the current in model L decreases by 0.5% at $t = 2$, 3.5% at $t = 4$ and 14% at $t = 8$. On average, the interface must be lower by similar amounts. The global volumes of the fluid in the current in model T and in the homogeneous $\beta = 0$ case are identical (the present approach discards the volume of the settled particles). Since the settling of the particles had little influence on the

https://doi.org/10.1017/S0022112098008878 Published online by Cambridge University Press

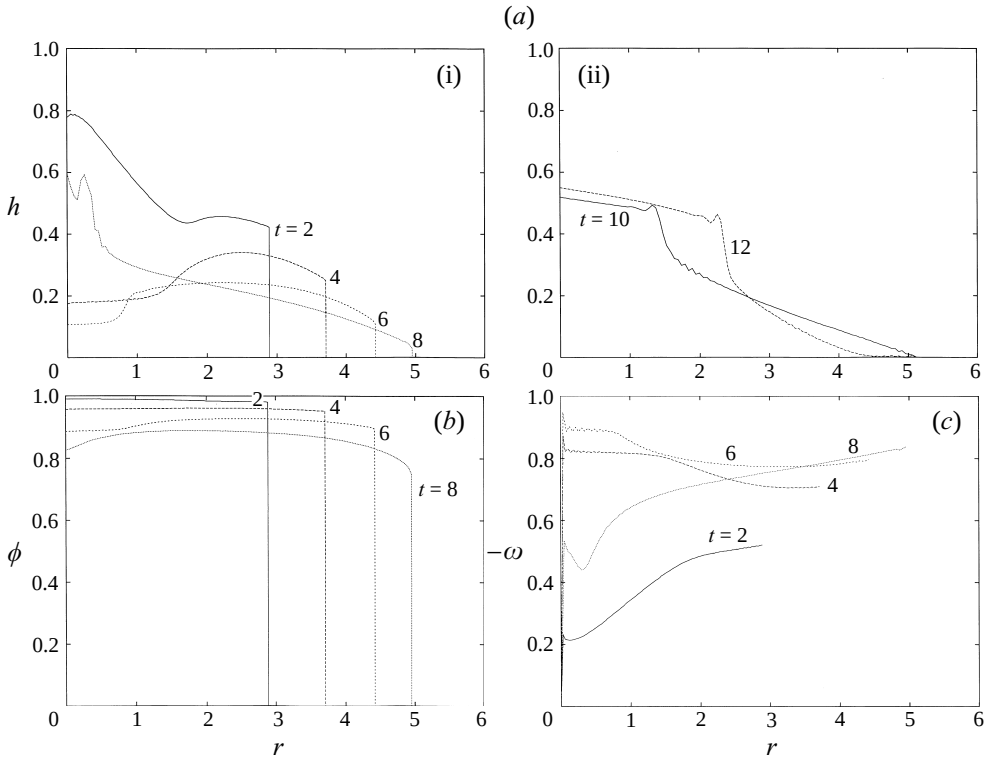


FIGURE 4. Rotating particle-driven current, model T. $\mathscr{C}^2 = 0.05$, other parameters as in figure 3. (*a*) (i, ii) Interface h vs. r, various t. (*b*) Particle volume-fraction ϕ vs. r, various t. (*c*) Angular velocity ω vs. r, various t.

position of the nose, the loci of the interfaces in model T and homogeneous $\beta = 0$ case are also very close. (Of course, at large t, say $\sim 1/\beta = 200$, the difference must be large since all the particles are expected to have settled out, while the homogeneous current maintains its density excess.)

The variation of the particle volume fraction according to model T is displayed in figure 4(*b*) (cf. figure 3*b*). The order of magnitude of the variations of ϕ with time are as in the non-rotating case, because the sedimentation itself is not influenced by Coriolis effects. However, the rotation modifies the r profile of this variable; in particular, the decay of ϕ near the nose increases with $\mathscr{C}$. This is a by-product of the faster decay of h_N in the rotating case, which influences the source term $-\beta\phi/h$ in the particle 'diffusion' equation (third equation in (2.19)).

The angular velocity in the current, $\omega = v/r$, is negative and of order of unity, as seen in figure 4(*c*). This means that the angular motion of the current lags considerably behind that of the ambient fluid (or the rotating frame of reference). As expected from the conservation of potential vorticity, ω and h are strongly connected. Roughly, $\omega \approx -1 + h$ in the interior, and $\omega \approx -1 + (r_0/r_N)^2$ near the nose. For $t \geqslant 4$ the angular velocity is smaller than -0.7 in the major part of the current, hence we may expect a large influence of the Coriolis terms. Indeed, this influence is represented by the $\mathscr{C}^2 r\omega(2+\omega)$ source term on the right-hand side of the radial momentum equation (2.19); for $\omega = -0.7$ the coefficient $|\omega(2+\omega)|$ attains 91% of its maximal value.

https://doi.org/10.1017/S0022112098008878 Published online by Cambridge University Press

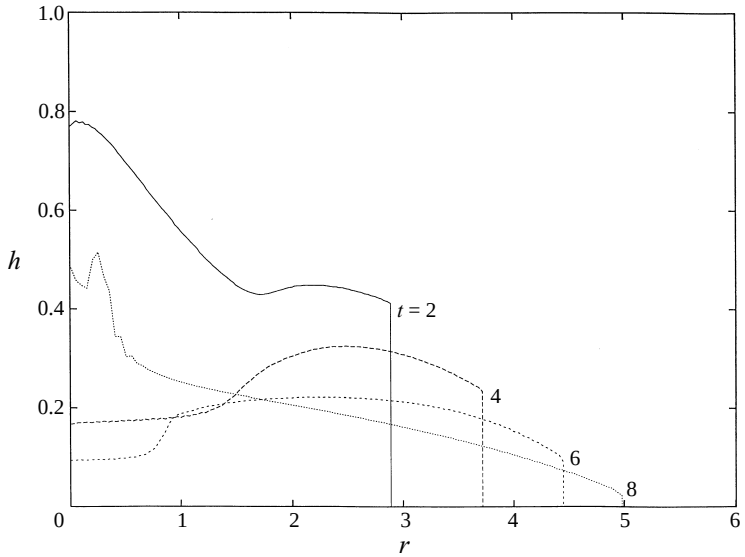


FIGURE 5. Rotating particle-driven current, model L, parameters as in figure 4. Interface h vs. r, various t.

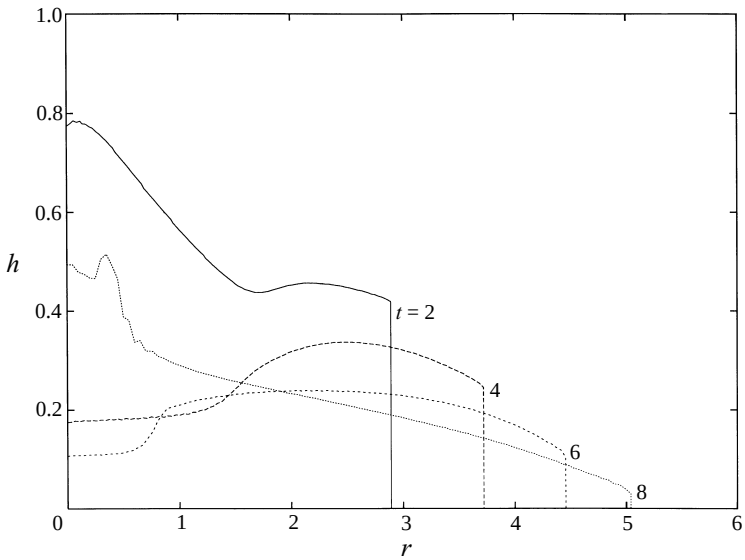


FIGURE 6. Rotating homogeneous ($\beta = 0$) current, other parameters as in figure 4. Interface h vs. r, various t.

The rotating current at its maximum propagation is close to – but not identical with – the SL, as seen from the comparison between figure 2 (with $\mathscr{C}^2 = 0.05$) and figure 4 (at $t \geqslant 8$). Both the shape of the interface and the angular velocity are essentially in agreement, but it is noted that the maximal r_N exceeds slightly the SL value, then starts to shrink, and the interface of the dynamic current at the corresponding time is not as smooth as in the SL. We speculate that the final adjustments of a dynamic current to the SL involves viscous effects, which were not incorporated in our models.

https://doi.org/10.1017/S0022112098008878 Published online by Cambridge University Press

The remarkable point, however, is that the current comes close to its SL in less than half a revolution of the system, $\mathscr{C}t/2\pi \approx 0.3$.

We summarize that the numerical solution of the equations of motion for the rotating gravity current, both particle-driven (models T and L) and homogeneous ($\beta = 0$), yield apparently meaningful and physically acceptable descriptions of the problem under investigation. The major Coriolis effects are quite similar for the particle-driven and homogeneous currents when $\beta \ll 1$. There are striking differences between non-rotating and rotating gravity currents. Other numerical computations, not discussed here, display the same consistent pattern. This suggests that a better understanding and interpretation may be gained by an asymptotic analysis for small values of $\mathscr{C}$ and β. Such an analysis is presented in the next section. The approximate analytical results also provide a verification of the numerical code.

Moreover, since the governing equations and boundary conditions contain approximations, experimental support is essential for the physical validation of the theoretical results. This aspect will be treated in §6.

5. Insights and approximations for $\mathscr{C}r_0 \ll 1$

When $\mathscr{C} \ll 1$ we expect, on account of the numerical results and order of magnitude considerations of the dominant dynamic balances, three major stages in the time-dependent behaviour of a gravity current.

(i) The Coriolis terms are much smaller than the inertial terms. An inertia–pressure balance prevails in the radial direction, and the current spreads as in the non-rotating $\mathscr{C} = 0$ case. However, due to the potential vorticity conservation, the angular velocity decreases substantially during this stage.

(ii) The Coriolis terms are of the order of magnitude of the inertial terms. A three-term Coriolis–inertia–pressure radial balance occurs. The current spreads more slowly than in the non-rotating case and its shape is modified from 'nose-up' to 'nose-down'.

(iii) The Coriolis terms are much larger than the inertial term. A radial balance between Coriolis effects and pressure gradient ensues. The radial velocity changes sign, and the height of the nose decreases to zero.

For clarity, we assume a homogeneous current, $\beta = 0$, $\phi = 1$. Afterwards, it will be shown that the discussion remains valid for $\beta \ll \mathscr{C}^2$ (the change of the volume fraction ϕ in the latter case will also be estimated).

5.1. *First stage*

Here we wish to substantiate the existence of the first stage and the emergence of the second stage.

In a non-rotating gravity current a 'long time' similarity solution exists, which is a good approximation for the real behaviour for $t > t_0 \approx 4r_0/Fr \gg 1$ (after a 'slumping' period see Huppert & Simpson 1980; Bonnecaze *et al.* 1995; Hallworth *et al.* 1996)†. In this solution r_N increases linearly with $t^{1/2}$. If the first stage exists for a rotating current with sufficiently small $\mathscr{C}$, the same 'long time' solution must be an accurate approximation for the radial motion, i.e. the Coriolis terms are expected to be a small perturbation of the similarity solution for some time interval in $t > t_0$. We therefore assume a solution of the form

$$h(t, y) = \dot{r}_N^2(t)H(y, t); \quad u(t, y) = \dot{r}_N(t)y. \tag{5.1}$$

† For definiteness, $r_N(t_0) = 3$.

https://doi.org/10.1017/S0022112098008878 Published online by Cambridge University Press

The essential boundary condition

$$u(y=1,t) = Fr[h(y=1,t)]^{1/2} \tag{5.2}$$

(hereafter Fr is a constant) is then simply reduced to

$$H(y=1,t) = Fr^{-2}. \tag{5.3}$$

Substituting (5.1) into the radial momentum equation,

$$u_t + h_r + uu_r = \mathscr{C}^2 r\omega(2+\omega), \tag{5.4}$$

we obtain

$$[\ddot{r}_N - \mathscr{C}^2 r_N \omega(2+\omega)]y + \frac{\dot{r}_N^2}{r_N}\frac{\partial H}{\partial y} = 0; \tag{5.5}$$

and into the continuity equation,

$$h_t + uh_r + hu_r + uh/r = 0, \tag{5.6}$$

we obtain

$$2H\dot{r}_N\ddot{r}_N + 2H\frac{\dot{r}_N^3}{r_N} + \dot{r}_N^2\frac{\partial H}{\partial t} = 0; \tag{5.7}$$

while the conservation of potential vorticity yields

$$\omega + \tfrac{1}{2}y\frac{\partial \omega}{\partial y} = -1 + \dot{r}_N^2 H(y,t) \tag{5.8}$$

with the condition

$$\omega(y=1,t) = -1 + [r_0/r_N(t)]^2. \tag{5.9}$$

Here H and r_0 are of order unity.

To describe the first stage, we let

$$r_N = Kt^{1/2}, \text{ and hence } \dot{r}_N = \tfrac{1}{2}Kt^{-1/2}, \quad \ddot{r}_N = -\tfrac{1}{4}Kt^{-3/2}, \tag{5.10}$$

where K is of order unity, as shown below.

We consider $t \gg 1$ (actually, $t > 4r_0/Fr$). First, using (5.8)–(5.10), we estimate that

$$\omega = -1 + O(t^{-1}), \quad \omega(2+\omega) = -1 + O(t^{-2}). \tag{5.11}$$

The momentum equation (5.5), on account of (5.10) and (5.11), yields, after some rearrangement,

$$\tfrac{1}{4}Kt^{-3/2}\left\{y[-1 + 4\mathscr{C}^2t^2(1+O(t^{-2}))] + \frac{\partial H}{\partial y}\right\} = 0; \tag{5.12}$$

and hence

$$H = Fr^{-2} + \tfrac{1}{2}[1 + O(\mathscr{C}^2t^2)](y^2 - 1). \tag{5.13}$$

Now in the continuity equation (5.7) the first two terms are $O(t^{-2})$ and cancel each other identically, while the third term is, relative to the previous ones, $O[\mathscr{C}^2t^2]$.

The global volume conservation,

$$2\pi\int_0^{r_N} rh\mathrm{d}r = 2\pi r_N\dot{r}_N^2\int_0^1 Hy\mathrm{d}y = \pi r_0^2 \tag{5.14}$$

gives the coefficient

$$K = 2[r_0^2Fr^2/(4 - Fr^2)]^{1/4}. \tag{5.15}$$

https://doi.org/10.1017/S0022112098008878 Published online by Cambridge University Press

The Coriolis terms in (5.13) give a relative contribution $O(Fr^2\mathscr{C}^2t^2)$ to (5.14).

We conclude that the Coriolis terms introduce $O(\mathscr{C}^2t^2)$ perturbations on the r, z, t non-rotating similarity profile of the gravity current. Thus, for large t and very small $\mathscr{C}t$ the non-rotating similarity solution for $r_N(t), h(r,t), u(r,t)$, supplemented by $\omega = -1$, approximate the motion. A relevant time interval for the first stage is therefore $t_0 < t < \mathscr{C}^{-1}$ which is feasible when $\mathscr{C}r_0 < Fr/4$. Hence, the existence of the first stage is expected even for moderately small values of $\mathscr{C}$, but a clear distinction between the first two stages requires $\mathscr{C} \ll Fr/(4r_0)$.

The physical interpretation of (5.12) is as follows. As the current spreads, its thickness decreases and, due to the nose condition $\dot{r}_N = Frh_N^{1/2}$, the speed of propagation is reduced. This deceleration, expressed by the inertial term in (5.12), is provided mainly by the gravity-induced pressure gradient, proportional to the inclination of the interface. Unlike the local inertial and gravity-induced pressure gradient, which decrease with time as the current becomes thinner, the Coriolis acceleration at a fixed radius remains practically constant (for $t \gg 1$). Hence its influence accumulates in time in spite of the small coefficient $\mathscr{C}^2$.

Actually, this Coriolis acceleration is equivalent to a radial pressure gradient in a non-rotating system. In a non-rotating frame of reference, the current (for $t \gg 1$) moves only in the radial direction, while the fluid above it is in solid-body rotation, and hence subject to $\mathrm{d}p/\mathrm{d}r = \mathscr{C}^2 r$. This pressure gradient is induced in the fluid of the current and seen, in the rotating frame, as the radial Coriolis term. Since the inertia and gravity-induced pressure gradient decay in time, the relative importance of the Coriolis term increases constantly. Therefore, the $\mathscr{C} = 0$ non-rotating solution is an approximation to the rotating gravity current which is non-uniform in time: at a sufficiently large t (actually, before the system performs one tenth of the first revolution, as shown below) significant Coriolis modifications of the non-rotating solution become necessary. This new stage is analysed below.

5.2. *Second stage*

The essential modifications are indicated by the foregoing balances. Obviously $\omega = -1$ is an accurate approximation. In the radial direction the need to decelerate the current remains. In this task, however, the gravity-induced pressure gradient, reproduced by $\partial H/\partial y$, is increasingly supplemented by the Coriolis term (or the centrifugally-induced pressure gradient). Consequently, we may expect two essential modifications of the non-rotating behaviour: (i) a stronger deceleration (slower propagation); and (ii) a reduction of $\partial H/\partial y$,

We found that these modifications start as small, $O(\mathscr{C}^2t^2)$, perturbations of the non-rotating similarity solution. Here we attempt to calculate in some detail these perturbations to leading order in $O(\mathscr{C}^2t^2)$.

We notice that this perturbation develops on a 'long time' coordinate,

$$\tau = \mathscr{C}t, \tag{5.16}$$

which actually has a simple physical interpretation: the time needs to be scaled with the angular period of the rotating frame (the first radian is attained at $\tau = 1$). Apparently, the initial Coriolis effect enters into the solution via even powers of τ. We therefore seek a solution of the form

$$r_N = Kt^{1/2}b^{-1/4}(\tau), \tag{5.17}$$

$$u = \dot{r}_N y + \tilde{u}(y, t, \tau), \tag{5.18}$$

https://doi.org/10.1017/S0022112098008878 Published online by Cambridge University Press

$$h = \dot{r}_N^2 H(y, t, \tau), \tag{5.19}$$

$$\omega = -1, \tag{5.20}$$

where

$$b(\tau) = 1 + 4\chi\tau^2, \quad \tilde{u} = BKt^{-1/2}\tau^2 y(1 - y^2), \tag{5.21}$$

with the dot denoting derivatives in time at fixed y, and K is the same constant as in the non-rotating case. Evidently, for $\mathscr{C} = 0$, the non-rotating similarity form is recovered, and for small τ, perturbations of $O(\tau^2)$ are introduced in r_N and u. Formally, a consistent correction $\tilde{\omega}$ could be incorporated into the right-hand side of (5.20). However, since the calculation of this variable is decoupled we shall discuss it separately below.

We remark that the profile of $\tilde{u}$ was inferred from a combination of analytical considerations of the Coriolis action and inspection of the numerical results. The modification function $b^{-1/4}(\tau)$ in (5.17), on account of (5.21), is a compact form for the expansion $1 - \chi\tau^2 + O(\tau^4)$; its non-uniqueness is not expected to alter the leading $O(\tau^2)$ term which is our major concern here in the following solution.

The task is to calculate the constant coefficients χ and B such that the perturbed similarity solution (5.17)–(5.21) satisfies the equation of motion when $\mathscr{C} > 0$ to higher accuracy than the original similarity solution, for τ small but finite. (Our attempt to reduce the error from $O(\tau^2)$ to $O(\tau^4)$ was only partly achieved, as described below; for a better formal result a more general dependency of $\tilde{u}$ on y should be assumed, but the resulting complication of the analysis is beyond the scope of this paper. The simplification is vindicated by the good agreement with numerical results, as discussed below.)

The 'nose condition' (5.2) reduces again to (5.3), which is an advantage of the attempted form (5.17)–(5.19).

We substitute (5.17)–(5.21) in the radial momentum equation and obtain, on the left-hand side, the same terms as in (5.5) plus

$$\dot{\tilde{u}} + (\dot{r}_N/r_N)\tilde{u} + (\tilde{u}\tilde{u}_y/r_N). \tag{5.22}$$

We realize that the last term is relatively $O(\tau^4)$, and therefore discard it. The remaining equation can be integrated, subject to (5.3), to give

$$H(y, \tau) = Fr^{-2} + \tfrac{1}{2}[1 + \psi(\tau)](y^2 - 1) - \tfrac{1}{4}\Upsilon(\tau)[y^2(2 - y^2) - 1], \tag{5.23}$$

where

$$\psi(\tau) = -4\tau^2[b^2(\tau) - 6\chi] \tag{5.24}$$

and

$$\Upsilon(\tau) = 2B\tau^2 b^{9/4}(\tau)[3 + b^{-1}(\tau)]. \tag{5.25}$$

We proceed to the continuity equation (5.6). On the left-hand side we obtain the same terms as in (5.7) plus

$$(\dot{r}_N^2/r_N)[\tilde{u}(\partial H/\partial y + H(\tilde{u}_y + \tilde{u}/y)]. \tag{5.26}$$

Using (5.23), we rearrange the left-hand side of (5.6) as

$$\frac{\text{LHS}(5.6)}{\frac{1}{4}K^2 t^{-2}} = 4[R(y) + O(\tau^4)], \tag{5.27}$$

https://doi.org/10.1017/S0022112098008878 Published online by Cambridge University Press

where

$$R(y) = -3\chi(2Fr^{-2}+1) + 1 + y^2(3\chi - 1) \\ + \tfrac{1}{4}B[4(1-y^2(2-y^2)) + y^2(1-y^2) + (2Fr^{-2} - 1 + y^2)(1-2y^2)]. \quad (5.28)$$

The rescaling with $\frac{1}{4}K^2t^{-2}$ was introduced to make the leading terms in the continuity equation, such as $2H\dot{r}_N\ddot{r}_N$, of order unity. Equation (5.27) displays the relative residue in the continuity equation. It is not possible to cancel $R(y)$ for $0 < y < 1$ as desired when χ and B are not both zero. However, we can impose on $R(y)$ two conditions that will make the solution meaningful. First, we require global volume conservation up to $O(\tau^4)$, which can be expressed as

$$\int_0^1 R(y)y\mathrm{d}y = 0, \quad (5.29)$$

and yields

$$B = -\tfrac{3}{2}(1 - \chi/\chi_0), \quad \chi_0 = \frac{1}{3}\frac{Fr^2}{4+Fr^2}, \quad (5.30)$$

for an arbitrary value of χ (physical considerations show that χ should be larger than 0 and smaller than χ_0). The second condition on $R(y)$ is less obvious. Here we chose to impose

$$\int_0^1 R(y)y^2\mathrm{d}y = 0, \quad (5.31)$$

which means that the volume influx weighted by the radius vanishes up to $O(\tau^4)$, and can also be interpreted as a restriction on the influx of radial momentum. Combined with (5.30) this produces

$$\chi/\chi_0 = f(Fr), \quad \text{with} \quad f(1.19) = 0.618, \quad f(0.72) = 0.774. \quad (5.32)$$

We note that, encouragingly, other reasonable conditions on $R(y)$, such as $R = 0$ at $y = 0$ or 1, give very similar results. For the results (5.30)–(5.32) and $Fr = 1.19$, $R(y)$ is indeed small, as seen in figure 7. Since no restriction was applied on the $O(\tau^4)$ term of (5.27), we expect that this term becomes locally dominant when $\tau^2 > |R(y)|$. Thus, for $\tau < 1$ the error in the continuity equation is controlled to be acceptably small: it behaves like τ^2 when τ is very small (say, < 0.1), and as τ^4 for larger values of this variable.

With the results (5.30)–(5.32) we also rechecked the global volume conservation (5.14). The relative error in this quantity can be expressed as

$$E = \left\{1 - \frac{Fr^2}{4-Fr^2}\left[\psi(\tau) - \tfrac{1}{3}\Upsilon(\tau)\right]\right\} b^{-3}(\tau) - 1 = A\tau^4 + O(\tau^6), \quad (5.33)$$

where the value of A is approximately 0.4 and 0.07 for $Fr = 1.19$ and 0.72, respectively. This suggests that the present approximate solution is substantially more accurate for the smaller value of Fr.

To summarize, the first and second stages are straightforwardly combined. For $4r_0/Fr < t < \mathscr{C}^{-1}$ and $\beta \ll \mathscr{C}^2$ the behaviour of the current is given by the approximation

$$r_N = Kt^{1/2}b^{-1/4}(\tau), \quad (5.34)$$

$$u = \tfrac{1}{2}Kt^{-1/2}b^{-5/4}(\tau)y\left[1 + 2B\tau^2 b^{5/4}(\tau)(1-y^2)\right], \quad (5.35)$$

$$h = \tfrac{1}{4}K^2t^{-1}b^{-5/2}(\tau)H(y,\tau), \quad (5.36)$$

https://doi.org/10.1017/S0022112098008878 Published online by Cambridge University Press

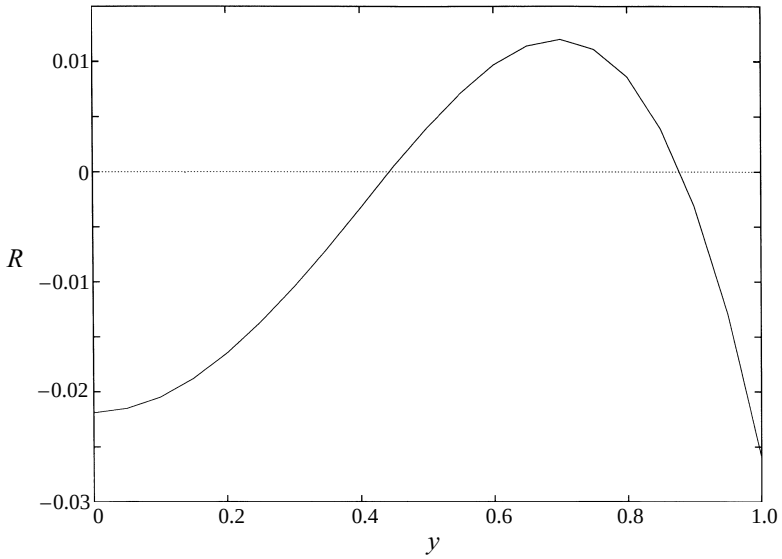


FIGURE 7. Residue $R(y)$ for $Fr = 1.19$, $\chi = 5.386 \times 10^{-2}$, $B = -0.573$ and $f(Fr) = 0.618$

$$H(y,\tau) = Fr^{-2} + \tfrac{1}{2}[1+\psi(\tau)](y^2-1) - \tfrac{1}{4}\Upsilon(\tau)[y^2(2-y^2)-1], \tag{5.37}$$

$$\omega = -1, \tag{5.38}$$

where

$$\tau = \mathscr{C}t, \tag{5.39}$$

$$b(\tau) = 1 + 4\chi\tau^2, \tag{5.40}$$

$$\psi(\tau) = -4\tau^2[b^2(\tau) - 6\chi], \tag{5.41}$$

$$\Upsilon(\tau) = 2B\tau^2 b^{9/4}(\tau)[3 + b^{-1}(\tau)]. \tag{5.42}$$

K, B and χ are constants; the first is given by (5.15), and

$$B = -1.5[1 - f(Fr)], \quad \chi = \frac{1}{3}\frac{Fr^2}{4+Fr^2}f(Fr), \tag{5.43}$$

with $f(Fr) = 0.6$ and 0.8 for $Fr = 1.19$ and 0.72, respectively. Recall that $\tau = 2\pi$ is the time for the first revolution of the system. A consistent correction for ω will be considered later.

This approximate solution has been validated by comparison with numerical results and good agreement was obtained. However, the initial conditions introduce some perturbations into the first stage which subsequently propagate into the second stage and obscure the comparison in the range of not very small $\mathscr{C}$. In other words, the accurate numerical attainment of the true asymptotic range $4r_0/Fr \ll t \ll 1/\mathscr{C}$ from standard initial conditions requires heavy computations with our scheme. This complication was readily avoided by using synthetic initial conditions, assuming the ideal accomplishment of the first stage as follows. We start at some specified $t = t_0$ $(1 < t_0 \ll 1/\mathscr{C})$ with $r_N(t_0)$ and $h(y,t_0)$ given by (5.17) and (5.19) and $\omega = -1$ is imposed for all y and t. The volume is also defined via a prescribed r_0. The subsequent behaviour, at least up to $\tau = 1$, was calculated for various values of $\mathscr{C}, Fr, r_0$, starting with the same $\tau_0^2 = \mathscr{C}^2 t_0^2 = 0.02$. (We note in passing that these

https://doi.org/10.1017/S0022112098008878 Published online by Cambridge University Press

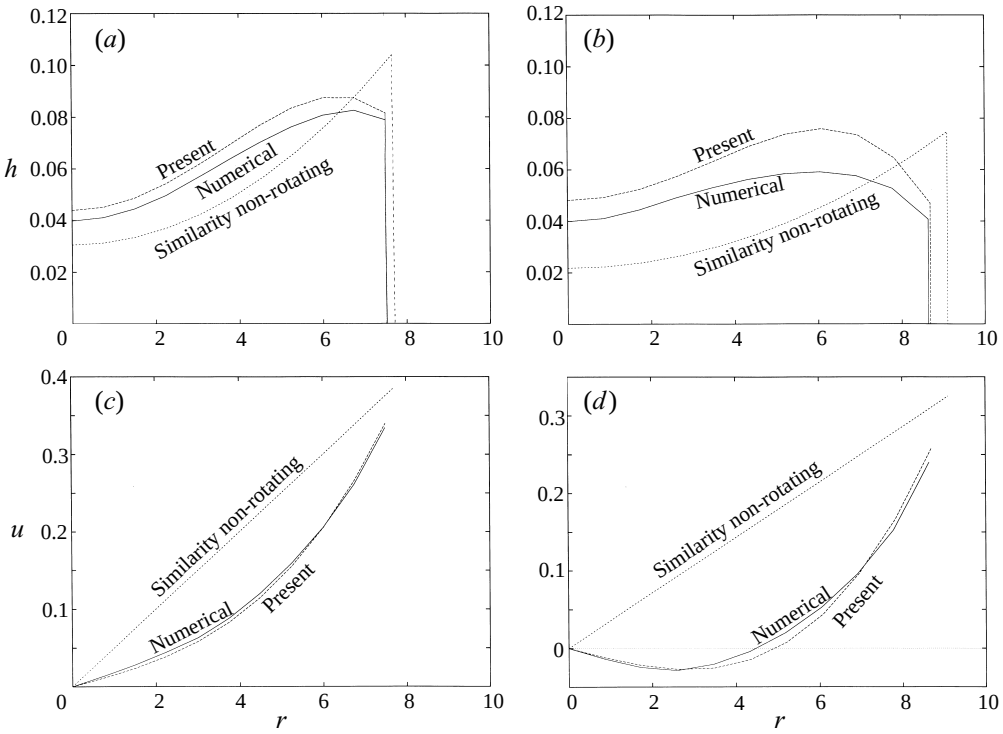


FIGURE 8. Comparison between numerical, similarity non-rotating, and present (asymptotic) solutions. (*a*) h vs. r at $t = 10$, $\tau = 0.707$, $Fr = 1.19$, $\mathscr{C}^2 = 0.005, \beta = 0$; (*b*) h vs. r at $t = 14$, $\tau = 0.990$; (*c*) u vs. r at $t = 10, \tau = 0.707$; (*d*) u vs. r at $t = 14$, $\tau = 0.990$.

smooth initial conditions also eliminate the spurious wiggles observed in the lock-release computations.)

In particular, runs with $\mathscr{C}^2 = 2\times10^{-2}, 0.5\times10^{-2}, 0.125\times10^{-2}$; $r_0 = 2$; and $Fr = 1.19$ were performed. Typical outcomes are shown in figure 8 (obtained with $f(Fr) = 0.6$). The results confirm the dependence of the Coriolis modifications on τ. For example, at $\tau = 0.707$ the computed $h(y = 1)$ is 24.5% below the non-rotating similarity value for all the above-mentioned values of $\mathscr{C}$ – although the corresponding times are $t = 5, 10, 20$; on the other hand, the difference of the computed value from the present approximate solution is only 3.2%. At $\tau = 1.131$ the computed r_N is 7% below the non-rotating similarity solution and 1% below the present solution.

Similar comparisons for $Fr = 0.72$, not displayed, yielded even better agreements.

As seen in this figure, the most striking effect of the Coriolis modifications is the change of the current's profile from 'nose up' to 'nose down'. The time for the first occurrence of this change, τ_1, can be calculated from the present solution as follows, see (5.19), (5.23), (5.24):

$$\frac{\partial H}{\partial y}(y = 1, \tau = \tau_1) = 0 = 1 + \psi(\tau_1), \tag{5.44}$$

and hence

$$\tau_1 \approx \frac{1}{2}\left[1 + \frac{Fr^2}{4 + Fr^2} f(Fr)\right]. \tag{5.45}$$

This prediction is confirmed by the numerical results. As time progresses the portion

https://doi.org/10.1017/S0022112098008878 Published online by Cambridge University Press

of the current with negative $\partial h/\partial y$ increases. The physical interpretation is as follows. The $\partial h/\partial y$ represents the pressure gradient induced by the buoyancy force. In the non-rotating case this is the means by which the tail of the current is decelerated to keep its velocity matched to that of the nose which is slowed down due to the decrease in its thickness, $\dot{r}_N = Fr[h_N(t)]^{1/2}$. In the rotating case the Coriolis effect also tends to decelerate the current. At small τ the Coriolis force 'helps' the above-mentioned conventional pressure gradient, therefore a reduction of $\partial h/\partial y$ occurs. At larger τ this Coriolis effect (which increases with r and is, locally, constant in time) provides more deceleration than the current needs to comply with the nose condition. This builds up fluid with negative $\partial h/\partial y$ behind the nose; in this region the gravity (buoyancy) pressure gradient tends to accelerate the fluid against the Coriolis effect.

Another noteworthy difference from the non-rotating current is the reversal of the radial velocity in the central region after some τ_2. According to (5.35) u becomes negative in the centre region $y^2 \ll 1$ for times larger than

$$\tau_2 \approx (-2B)^{-1/2} \approx 0.9 \text{ for } Fr = 1.19 \\ \approx 1.2 \text{ for } Fr = 0.72. \tag{5.46}$$

The region of negative u is expected to expand rapidly with τ. Although already in the speculative range of τ, this prediction is in excellent agreement with the numerical results, see figure 8(d) (for this run no negative u was recorded for $\tau < 0.85$).

Finally, we use the second stage approximation to illuminate the transition to the possible steady-state lens shape (SL) discussed in §3. It turns out that the SL radius, $(2r_0)^{1/2}\mathscr{C}^{-1/2}$, is first reached, according to (5.17), at

$$\tau_3 \approx \frac{1}{Fr}(1 - \tfrac{1}{8}Fr^2). \tag{5.47}$$

We also estimate

$$h_N(\tau_3) \approx \tfrac{1}{2}(1 + \tfrac{1}{4}Fr^2)\mathscr{C}r_0 b^{-5/2}(\tau). \tag{5.48}$$

At this instant the current still propagates forward with a nose velocity only about 10% smaller than in a non-rotating case. We must therefore infer that the current will initially spread beyond the SL radius, then shrink back. This expectation is consistent with the observation that an increasing part of the current acquires negative u for $\tau > \tau_2$. Remarkably, the values of τ_3 and τ_2 are close. We may roughly say that when the current first passes the SL radius, a returning motion starts to build up, which is enhanced with further spread.

The appearance of this reverse motion seems to mark the end of the second stage, and the beginning of the third stage in which the motion is governed by a Coriolis–pressure balance, with small contributions from the inertial term.

5.2.1. *The correction to* $\omega = -1$

With the previously obtained $r_N(t), H(y,t,\tau)$ the correction to the value of ω, so far considered $= -1$ to leading order, can be considered with the use of (5.8)–(5.9). Letting

$$\omega = -1 + \tilde{\omega}(Y,t,\tau), \quad \text{where} \quad Y = y^2, \tag{5.49}$$

we obtain

$$Y\frac{\partial \tilde{\omega}}{\partial Y} + \tilde{\omega} = \dot{r}_N^2(t)H(Y,t,\tau), \tag{5.50}$$

subject to

$$\tilde{\omega}(Y = 1) = [r_0/r_N(t)]^2. \tag{5.51}$$

https://doi.org/10.1017/S0022112098008878 Published online by Cambridge University Press

The analytical solution is cumbersome, but approximations for $Y \ll$ and $Y \to 1$ give some useful insights. In the former region (for, say, $Y < 0.8$) the derivative term is discarded, which yields simply that

$$\tilde{\omega} = h(Y, t, \tau). \tag{5.52}$$

In the latter region we freeze the space-dependent terms in (5.50) at $Y = 1$, and determine, after linearization and rearrangement, that

$$\tilde{\omega} \approx [r_0/r_N(t)]^2\{1 + [1 - (r_N(t)\dot{r}_N(t)/r_0 Fr)^2](1 - Y)\}. \tag{5.53}$$

This result indicates that for small τ the maximum value of $\tilde{\omega}$ is at the nose, but later on (from around $\tau = 0.5$) a small decrease of $\tilde{\omega}$ from the interior to the nose occurs. Evidently, in the interior and near the nose $\tilde{\omega} = O(t^{-1})$, as assumed in the foregoing analysis.

5.3. *The change of ϕ in a particle-driven current*

The previous analysis was performed for the homogeneous current case, $\beta = 0$. However, it can be used, without loss of formal accuracy, for the particle-driven case with $\beta \ll \mathscr{C}^2$. This is justified by the behaviour of the volume fraction, $\phi(y, t)$, for which we now derive an approximation. We assume an expansion of the form

$$\phi = 1 - \beta\tilde{\phi}(y, t) + O(\beta^2), \tag{5.54}$$

and assume further that $\beta\tilde{\phi}$ is sufficiently small to affect only slightly the Coriolis-perturbed flow discussed above during any instant in the entire interval $0 < \tau < 1$. An inspection of the equations of motion shows that the straightforward restriction can be expressed as

$$\beta\tilde{\phi}(y, \tau) \ll \tau^2. \tag{5.55}$$

In this case, we can attempt to evaluate the perturbation $\tilde{\phi}$ from the particle-continuity equation (2.19)

$$\phi_t + u\phi_r = -\beta\phi/h, \tag{5.56}$$

with u and h given to leading order by (5.18) and (5.19). This yields

$$\dot{\tilde{\phi}} + \tilde{u}\tilde{\phi}_y = 1/\dot{r}_N^2 H(y, \tau) + O(\beta); \tag{5.57}$$

and with the substitution of (5.21) and (5.36)

$$\dot{\tilde{\phi}} + [KBt^{-1/2}\tau^2 y(1 - y^2)]\tilde{\phi}_y = \left(\frac{2}{K}\right)^2 tb^{5/2}(\tau)\frac{1}{H(y, \tau)}. \tag{5.58}$$

This is more conveniently expressed in terms of $Y = y^2$ and $\tau = \mathscr{C}t$ as

$$\frac{\partial\tilde{\phi}}{\partial\tau} + \mathscr{B}\tau^{3/2}Y(1 - Y)\frac{\partial\phi}{\partial Y} = \left(\frac{2}{\mathscr{C}K}\right)^2 \tau b^{5/2}(\tau)\frac{1}{H(Y, \tau)}, \tag{5.59}$$

subject to the condition $\tilde{\phi}(y, \tau = 0) = 0$, where

$$\mathscr{B} = 2KB\mathscr{C}^{-1/2}. \tag{5.60}$$

The solution is obtained by the method of characteristics,

$$\frac{\mathrm{d}\tilde{\phi}}{\mathrm{d}\tau} = \left(\frac{2}{\mathscr{C}K}\right)^2 \tau b^{5/2}(\tau)\frac{1}{H(Y, \tau)} \tag{5.61}$$

https://doi.org/10.1017/S0022112098008878 Published online by Cambridge University Press

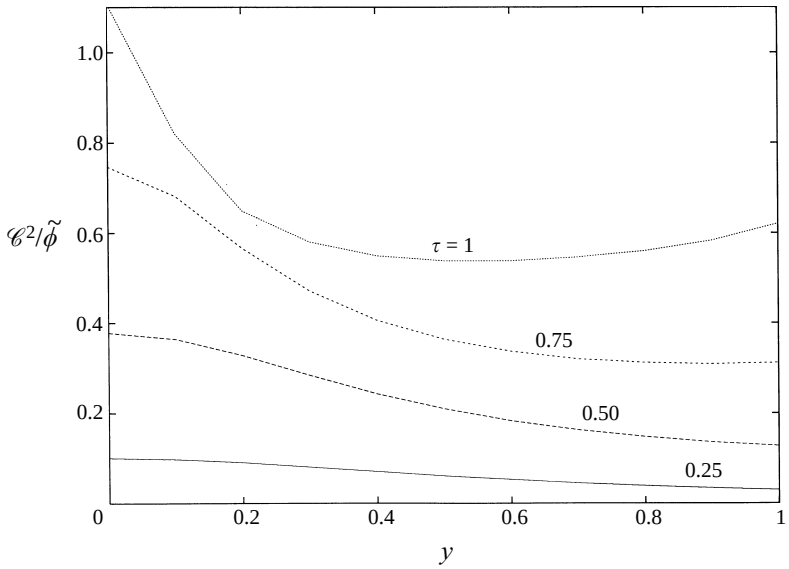


FIGURE 9. $\tilde{\phi}\mathscr{C}^2$ vs. y for various τ, $\mathscr{C}^2 = 0.005$, $r_0 = 2$, $Fr = 1.19$.

on

$$\frac{\mathrm{d}Y}{\mathrm{d}\tau} = \mathscr{B}\tau^{3/2} Y(1 - Y). \tag{5.62}$$

From the last equation we obtain the characteristic that reaches the position Y_1 at τ_1

$$Y_c(\tau) = \frac{C_1 \exp(\frac{2}{5}\mathscr{B}\tau^{5/2})}{1 + C_1 \exp(\frac{2}{5}\mathscr{B}\tau^{5/2})}, \tag{5.63}$$

where

$$C_1 = [Y_1/(1 - Y_1)] \exp(-\tfrac{2}{5}\mathscr{B}\tau_1^{5/2}). \tag{5.64}$$

Combining (5.61) and (5.62) with (5.63), we obtain the value of $\tilde{\phi}$ at a chosen Y_1, τ_1 as

$$\tilde{\phi}(Y_1, \tau_1) = \left(\frac{2}{\mathscr{C}K}\right)^2 \int_0^{\tau_1} \frac{\tau b^{5/2}(\tau)\mathrm{d}\tau}{H[Y_c(\tau), \tau]}. \tag{5.65}$$

(To be more explicit, $H[Y_c, \tau]$ means that in (5.37) y^2 is replaced by the expression (5.63).) Since H and b are both of order unity in the range of interest, we expect $\tilde{\phi} \sim \tau^2/\mathscr{C}^2$. Hence the restriction (5.55) can be satisfied when $\beta \ll \mathscr{C}^2$, in which case the present approximation is validated. We note that for $Y_1 = 0$ and $Y_1 \to 1$ we obtain $Y_c = 0$ and 1 respectively, and (5.65) reduces to the usual boundary conditions applied at these positions.

The numerical integration of (5.65) is straightforward; typical results are presented in figure 9. The integrand depends on the parameters Fr, r_0 and $\mathscr{C}$ so that a general solution of (5.65) is not available.

We note that the type of approximation used in the derivation of $\tilde{\phi}$ in the rotating gravity current may be used also in the non-rotating case for the extension of the similarity solution to a particle-driven current. This topic will be discussed elsewhere (Hogg, Ungarish & Huppert 1998).

https://doi.org/10.1017/S0022112098008878 Published online by Cambridge University Press

5.4. *Third stage*

The approximations used for the analysis of the first and second stages are not valid in this stage, formally because the boundary condition (5.3) is incompatible with the expectation that $h(r_N)$ becomes zero at a finite τ. An estimate of the propagation of the current in this stage may be obtained by considering the balances on characteristics, and, of course, from the numerical results. These indicate that the current propagates slowly, in a time interval $\Delta\tau \sim 1$, to about 35% beyond the SL radius, where the height of the nose becomes zero. We expect that it will subsequently shrink back to the SL radius, but our inviscid model and nose conditions are not expected to remain accurate for these circumstances. This topic is left for future investigation.

6. Experimental observations

The theoretical analysis was tested by several visualization tests. The apparatus consisted of a cylindrical container of radius 45 cm with transparent sidewalls, which can be set in rotation about the vertical axis, z. The free surface of the fluid was open to the atmosphere. The 'lock' from which the current was released was a small inner cylinder of inner radius 4.7 cm, wall thickness of 0.3 cm and height 15 cm. This was placed in a central position on the bottom of the container by means of an elastic seal (a heavy metal ring on the upper side of the inner cylinder was used to increase the pressure on the seal). The inner cylinder could be lifted with the aid of a simple mechanism of strings and pulleys. A metal frame attached to the rotating container supported cameras and the above-mentioned mechanism. Observation was possible from both above and the side. A video camera, co-rotating with the container, recorded the view from above.

For a typical test, the container was filled with tap water to a height of 10 cm. The inner (top- and bottom-less) cylinder was lowered and sealed to the bottom. A measured amount of salt or heavy particles was added to the water in the inner cylinder, plus 2 cm^3 of dye. This coloured mixture made up the heavier intruding fluid. The system was rotated at some pre-assigned angular velocity, and the fluids allowed to spin-up for about 15 min. The experiment started with the quick lifting of the inner cylinder ('lock'), which released the coloured heavy mixture into the ambient transparent water. Unfortunately, not many details could be seen because, typically, the time of propagation was only about 10 s and after the first 2 s the average thickness of the current became less then 1 cm. For better results a considerably larger container and/or more sophisticated release and recording means are necessary.

The propagation of the nose, $r_N(t)$, was extracted from the video camera records, using a pre-marked grid of concentric circles (radii 5, 10, ...40 cm) on the bottom of the container. The current's front had some asymmetries and ragged portions (due to perturbations and wall shear during the release stage) and we used some intuitive 'smoothing' to track the nose.

The range of tested parameters was, approximately: $h_0 = 10$ cm, $r_0 = 0.47$ (in dimensionless form), $g_0' = 20$–80 cm s^{-2} and $\Omega = 0.2$–0.5 s^{-1}. The inertial time scales, $(h_0/g_0')^{1/2}$, were 0.71–0.35 s. The corresponding spin-up intervals, $2h_0/(\nu\Omega)^{1/2}$, were 7.4–4.8 min, and the length scales of the Ekman layer were 0.22–0.14 cm. Note that when the current attains the radius $r_N \approx 25$ cm its average thickness, $h_0(r_0/r_N)^2$, is about twice the Ekman layer length scale.

The observed currents were stable. (We recall that instabilities of a closely related 'bottom' vortex are expected for $\mathscr{C}r_0 > 0.375$, see Saunders 1973.) The simple release

https://doi.org/10.1017/S0022112098008878 Published online by Cambridge University Press

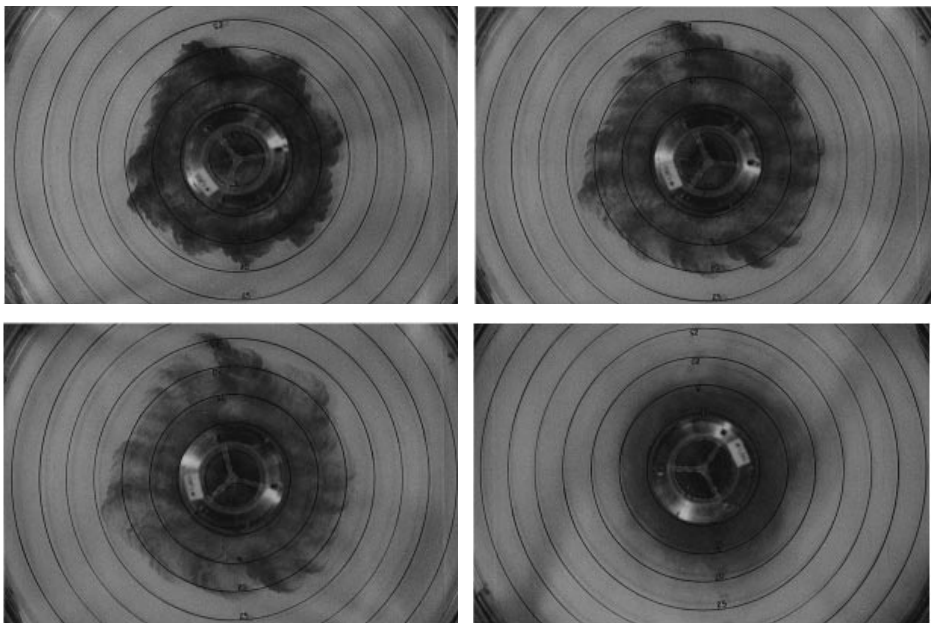


FIGURE 10. Photographs from above of the propagation of a saline current in the rotating cylinder, $\mathscr{C}^2 = 0.10$. $g_0' = 20$ cm s^{-2}. Time increases from photo 1 to photo 4.

mechanism caused some initial perturbations in the current and ambient fluid and this was reflected by deviations from the symmetrical pattern and some ragged portions of the interface, which persisted during the stage of propagation. These features appeared both in the non-rotating and rotating tests. However, no relative amplification or break-ups occurred; in contrast, in the rotating cases some decay of these asymmetries was observed close to and after the attainment of the maximum radius. Representative behaviour is displayed in figure 10.

The numerical results used for comparison were obtained with $\mathscr{H} = 1$ in the boundary condition (2.36), i.e. the initial height of the current equals that of the ambient fluid.

Saline-driven current results are shown in figure 11. To emphasize the Coriolis effects the non-rotating $\mathscr{C} = 0$ case is also displayed.

For $\mathscr{C} = 0$ the theoretical propagation is faster than the measured one (except for the first recorded point). This discrepancy may be attributed to the viscous effects and the reverse motion in the ambient fluid which have been neglected in the model.

For $\mathscr{C} > 0$ the theoretical propagation, both forwards and backwards, is faster than the measured one (except for the first recorded points). For the forward propagation the foregoing explanation for the discrepancy applies. As predicted by theory, r_N reaches a maximum whose value is in fair agreement with the experiment. However, the backward shrink of the observed current to the SL radius is significantly slower and less clear-cut than in the theory. This may be attributed to the Ekman-type balance between Coriolis and viscous terms that is expected to appear in the experiment when the current reaches its maximum r_N. This thickness of the current is about that of an Ekman layer; hence an Ekman-type smoothing of the angular velocity difference (between the current and the boundary) is expected to occur on the time scale $2\Omega^{-1} \sim 5$ s. This lessens the Coriolis effect imposed by the outer fluid on the current.

https://doi.org/10.1017/S0022112098008878 Published online by Cambridge University Press

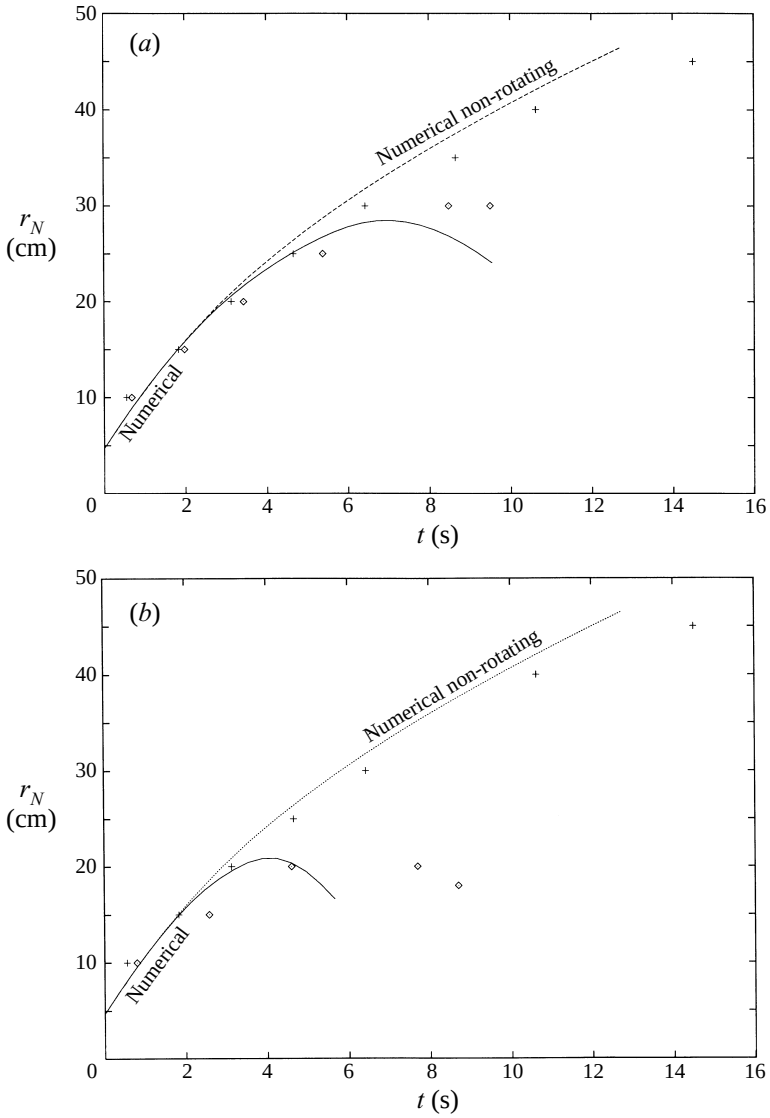


FIGURE 11. Saline-driven current, r_N vs. t, numerical results and experiments for (*a*) $\mathscr{C}^2 = 0.028$, (*b*) 0.10 ($\diamond$), and non-rotating + case. $g_0' = 20$ cm s^{-2}.

The experiments with a suspension rather than with a saline solution were less conclusive. We used silicon carbide particles ($\rho_p = 3.22$ g cm^{-3}) of average diameter 9×10^{-4} cm, whose Stokes settling velocity is 1.0×10^{-2} cm s^{-1}. The typical tests were performed with $g_0' = 20$ cm s^{-2} and $\Omega = 0.46$ s^{-1}, hence $\beta = 0.7 \times 10^{-3}$ and $\mathscr{C}^2 = 0.1$.

The major complication encountered was that in the inner cylinder ('lock'), while the suspension was being spun-up (the relevant time interval $2h_0/(\nu\Omega)^{1/2}$ is about 5 minutes) significant settling of particles occurred before the suspension was released into the ambient. Moreover, it appears that the Ekman layer pumping during the spin-up process modifies the conventional gravitational settling and disturbs the homogeneous particle distribution. Consequently, the theoretical initial conditions of a homogeneous suspension in solid-body rotation in the domain $0 < r < r_0$, $0 < z < 1$

https://doi.org/10.1017/S0022112098008878 Published online by Cambridge University Press

could not be well approximated. Even after some attempts to compensate for the particle settling by starting the spin-up with a higher cylinder of suspension, the satisfactory initial conditions could not be attained. This made reliable quantitative comparisons impossible. However, there was qualitative agreement between theory and observations. For the particle-driven case we noticed a higher tendency for instability and lens break-up than in the saline case. This may be a consequence of the incomplete spin-up and inhomogeneous particle distribution in the suspension domain prior to release into the ambient. The problem of combined spin-up and settling in the suspension, and the possible effects on the particle-driven current generated after the action of such a combination in the 'lock' domain, requires a special analysis that is beyond the scope of this work.

The experiments confirm the theory concerning the essential differences between the non-rotating and rotating axisymmetric currents even for small values of $\mathscr{C}$ ($\mathscr{C}r_0 = 0.08$ in figure 11), and the influence of the parameter $\mathscr{C}$ on the behaviour of a rotating current. In particular, the present model seems to be a fairly accurate predictive tool upon the incorporation of the hypothesis that the non-rotating nose condition $\dot{r}_N = Fr(\phi h)^{1/2}$ remains valid (here with the specific form (2.36), at least for small values of $\mathscr{C}$).

However, more complex experiments in a much larger container seem to be necessary for a more rigorous confirmation (and perhaps improvement) of the theory. In particular, it would be useful to increase the average thickness considerably above that of the Ekman layers during all stages of propagation, and to obtain good records of $h(r)$ at various times. This will throw more light on the Coriolis effects on the nose condition.

7. Concluding remarks

This study has pointed out some essential features of an axisymmetric particle-driven gravity current in a rotating frame. The theoretical description used the one-layer inviscid shallow-water equations, in a very deep solid-body rotating ambient, which were solved numerically and asymptotically for small $\mathscr{C}$ (ratio of Coriolis to inertial effects) and β (dimensionless settling velocity of particles). The required correlation for the nose velocity was assumed to be as in the non-rotating circumstances. The homogeneous current was treated as a particular case, $\beta = 0$. The results were corroborated by simple experiments. The closest study for a similar non-rotating current is that by Bonnecaze *et al.* (1995).

The most striking differences from the current in a non-rotating, $\mathscr{C} = 0$, frame appear up in the shape of the interface (thinner at the nose than at the tail) and in the restricted radius of propagation (about $\mathscr{C}^{-1/2}$ times the initial radius).

For small values of $\mathscr{C}$ and β, three major stages may be distinguished in the motion of the current. (i) In about the first initial tenth of a revolution, the current spreads radially almost as in a non-rotating frame, but its angular velocity decreases significantly. (ii) In the subsequent tenth of a revolution the radial velocity decelerates rapidly, and the interface develops a new shape, thinner at the nose and thicker at the tail, The radius of propagation reaches that of a steady-state lens (SL) but continues to grow. (iii) The current propagates slowly, overshoots the SL radius by about 35% while the height of the head decreases to zero, then shrinks back. This stage, which takes about one fifth of a revolution, requires additional study because it involves effects (such as viscosity) which were not included in the analysis. The formation of the SL may be considered, theoretically, the end of the current process.

https://doi.org/10.1017/S0022112098008878 Published online by Cambridge University Press

In practice, however, the SL is only a quasi-steady stage. Sedimentation of particles and/or viscous spin-up and/or instabilities will dissipate the SL into the ambient after some additional (sometimes many) revolutions.

The present study provides an additional dynamical link for the formation of oceanic structures called rings, eddies or vortices from simple initial conditions.

Each particular result (i.e. for a certain combination of the dimensionless parameters) presented in the paper can actually be extended to a family of cases by a simple similarity rescaling of the variables; this, together with a simple 'box model' for the approximate description of the main effects detected in the present study, are discussed in Ungarish & Huppert (1998).

Several interesting extensions are left for future work, such as a two-layer model, and the incorporation of viscous effects (the Ekman layer correlations seem to be adequate for the first approximation). The Coriolis influence on the nose velocity correlation, which is a major bottleneck for accurate modelling, so far has received very little attention. The possibility of reverse motion, after the overshoot of the SL radius, is a complication with no counterpart in a non-rotating current. It appears that most of the required information, like in the non-rotating circumstances, must be acquired by experimental work. This would necessitate experiments in a rotating container considerably larger than the one available in our laboratory (whose diameter is 90 cm).

We wish to thank Mr M. A. Hallworth for essential assistance in the experimental work, and Dr J. R. Lister for useful comments and suggestions. The research was supported by the EPSRC.

Appendix. On the z-averaged equations

Some details of the derivation of the z-averaged equations of motion of the current in $0 \leqslant z \leqslant h(r,t)$ are briefly presented.

Consider first the interface $\Sigma : h(r,t) - z = 0$, between the current (suspension) and the ambient pure fluid. The motion is prescribed by the equation (see, for example, Ungarish 1993, §2.3)

$$\frac{\partial h}{\partial t} + u_p(z=h)\frac{\partial h}{\partial r} - w_p(z=h) = 0, \tag{A 1}$$

or

$$\frac{\partial h}{\partial t} + u(z=h)\frac{\partial h}{\partial r} - w(z=h) = -[u_p(z=h) - u(z=h)]\frac{\partial h}{\partial r} + [w_p(z=h) - w(z=h)]. \tag{A 2}$$

The last term on the right-hand side introduces the difference between the models T and L. In model T it is assumed that there is no relative velocity between the particles and the fluid on the interface, and hence the right-hand side of (A 2) vanishes. In model L it is assumed that the settling of the particles relative to the fluid on the interface is as in a quiescent fluid, i.e. given by the Stokes velocity in the vertical direction only (approximately), or equal to $-\beta$ in dimensionless form.

If we use (averaged) values of u, not dependent on z, with $w(z=0) = 0$, and express $w(z=h)$ in terms of $u(r,t)$ with the aid of the continuity equation, we obtain from (A 2), in dimensionless form

$$\frac{\partial h}{\partial t} + \frac{1}{r}\frac{\partial}{\partial r}ruh = \begin{cases} 0, & \text{T model} \\ -\beta, & \text{L model.} \end{cases} \tag{A 3}$$

https://doi.org/10.1017/S0022112098008878 Published online by Cambridge University Press

We obtain the driving pressure gradient in the current using (2.10),

$$\int_0^h \frac{\partial p}{\partial r}\mathrm{d}z = \rho_a \Omega^2 r h + \rho_i g \left[\left(1 - \frac{\rho_a}{\rho_i} + \varepsilon\alpha\right)\frac{1}{2}\frac{\partial}{\partial r}h^2 + \varepsilon\frac{\partial \alpha}{\partial r}\tfrac{1}{2}h^2\right],$$

which can be rewritten as

$$\int_0^h \frac{\partial p}{\partial r}\mathrm{d}z = \rho_a \Omega^2 r h + \rho_i g_0' \left[\frac{1}{2}\frac{\partial}{\partial r}(\phi - \gamma)\, h^2\right]. \tag{A 4}$$

Now we reconsider the momentum equation for model T. (The extension to model L is straightforward.) Subsequently, we assume (averaged) values of u and v, not dependent on z, with $w(z = 0) = 0$.

Integrate the right-hand side of (2.5) from 0 to h, use (A 2) and (A 4), and divide by ρ_i to obtain

$$(1+\varepsilon\alpha)\left[\frac{\partial}{\partial t}uh + \frac{1}{r}\frac{\partial}{\partial r}ru^2 h\right] + g\varepsilon\alpha_0 \frac{\partial}{\partial r}\left[\tfrac{1}{2}(\phi-\gamma)h^2\right] - (1+\varepsilon\alpha)vh\left(2\Omega + \frac{v}{r}\right) = \Omega^2 r\varepsilon\alpha_0(\phi-\gamma)h. \tag{A 5}$$

Hereafter we switch to dimensionless form: scale length with h_0, time with $(h_0/g_0')^{1/2}$, u with $(h_0 g_0')^{1/2}$ and v with $\mathscr{C}(h_0 g_0')^{1/2}$.

Since $\varepsilon\alpha_0 \ll 1$, we discard $\varepsilon\alpha$ as compared to 1, and assume that, formally, $\mathscr{C}^2 \gg \varepsilon\alpha_0$. Equation (A 5) gives

$$\frac{\partial}{\partial t}uh + \frac{1}{r}\frac{\partial}{\partial r}ru^2 h + \frac{\partial}{\partial r}\left[\tfrac{1}{2}(\phi-\gamma)h^2\right] - \mathscr{C}^2 vh\left(2 + \frac{v}{r}\right) = \varepsilon\alpha_0\mathscr{C}^2(\phi-\gamma)hr. \tag{A 6}$$

The centrifugal (last) term is neglected as compared with the Coriolis term.

The integral of (2.6) from 0 to h, using the dimensionless variables, yields

$$\frac{\partial vh}{\partial t} + \frac{1}{r}\frac{\partial}{\partial r}ruvh + uh\left(2 + \frac{v}{r}\right) = 0. \tag{A 7}$$

Finally, we consider the particle continuity equation, for the z-averaged variables. Since particles settle out only at the bottom with velocity β, this is (for both T and L models)

$$\frac{\partial \phi h}{\partial t} + \frac{1}{r}\frac{\partial}{\partial r}ru\phi h = -\beta\phi. \tag{A 8}$$

Expansion and use of (A 3) yields

$$\frac{\partial \phi}{\partial t} + u\frac{\partial \phi}{\partial r} = -\frac{\phi}{h}\left[\beta - \left(\frac{\partial h}{\partial t} + \frac{1}{r}\frac{\partial}{\partial r}ruh\right)\right] = \begin{cases} -\phi\beta/h, & \text{in model T} \\ 0 & \text{in model L.} \end{cases} \tag{A 9}$$

REFERENCES

Anderson, D. A., Tannehill, J. C. & Pletcher R. M. 1984 *Computational Fluid Mechanics and Heat Transfer*. Hemisphere.

Benjamin, T. B. 1968 Gravity currents and related phenomena. *J. Fluid Mech.* **31**, 209–248.

Bonnecaze, R. T., Huppert, H. E. & Lister, J. R. 1993 Particle-driven gravity currents. *J. Fluid Mech.* **250**, 339–369.

Bonnecaze, R. T., Hallworth, M. A., Huppert, H. E. & Lister, J. R. 1995 Axisymmetric particle-driven gravity currents. *J. Fluid Mech.* **294**, 93–121.

Chen, J. C. 1980 Studies on gravitational spreading currents. PhD thesis, California Inst. Tech.

Csanady, G. T. 1979 The birth and death of a warm core ring. *J. Geophys. Res.* **84**, 777–780.

Einstein, H. 1968 Deposit of suspended particles in a gravel bed. *J. Hydraul. Div. ASCE* **94**, 1197–1205.

https://doi.org/10.1017/S0022112098008878 Published online by Cambridge University Press

GRUNDY, R. E. 1986 Self-similar solutions of the shallow-water equations representing gravity currents with variable inflow. *J. Fluid Mech.* **169**, 337–351.

FLIERL, G. R. 1979 A simple model for the structure of warm and cold core rings. *J. Geophys. Res.* **84**, 781–785.

GRIFFITHS R. W. & HOPFINGER E. J. 1983 Gravity currents moving along a lateral boundary in a rotating fluid. *J. Fluid Mech.* **134**, 357–399.

GRIFFITHS R. W. 1986 Gravity currents in rotating systems. *Ann. Rev. Fluid Mech.* **18**, 59–89.

GRIFFITHS R. W. & LINDEN P. F. 1981 The stability of vortices in a rotating, stratified fluid. *J. Fluid Mech.* **105**, 283–316.

HALLWORTH, M. A., HUPPERT, H. E., PHILLIPS, J. C. & SPARKS, R. S. 1996 Entrainment into two-dimensional and axisymmetric turbulent gravity currents *J. Fluid Mech.* **308**, 289–311.

HOGG, A., UNGARISH, M. & HUPPERT H. E. 1998 Asymptotic solutions for particle-driven gravity currents (in preparation).

HOULT, D. P. 1972 Oil spreading on the sea. *Ann. Rev. Fluid Mech.* **4**, 341–368.

HUPPERT H. E. & SIMPSON, J. E. 1980 The slumping of gravity currents, *J. Fluid Mech.* **99**, 785–799.

MARTIN, D. & NOKES, R. 1988 Crystal settling in a vigorously convecting magma chamber. *Nature* **332**, 543–536.

RICHARDSON, P. L. 1983 Gulf stream rings. In *Eddies in Marine Science* (ed. A. R. Robinson). Springer.

SAUNDERS, P. M. 1973 The instability of a baroclinic vortex. *J. Phys. Oceanogr.* **3**, 61–65.

SIMPSON, J. E. 1997 *Gravity Currents in the Environment and the Laboratory*. Cambridge University Press.

SPARKS, R. S. J., BONNECAZE, R. T., HUPPERT, H. E., LISTER, J. R., HALLWORTH, M. A., MADER, H. & PHILLIPS, J. C. 1993 Sediment-laden gravity currents with reversing buoyancy. *Earth. Planet. Sci. Lett.* **114**, 243–257.

UNGARISH, M. 1993 *Hydrodynamics of Suspensions*. Springer.

UNGARISH, M. & HUPPERT, H. E. 1998 Simple models of Coriolis-influenced axisymmetric particle-driven gravity currents. *Intl J. Multiphase Flow* (submitted).

https://doi.org/10.1017/S0022112098008878 Published online by Cambridge University Press